Engineering Science and Technology, an International Journal 48 (2023) 101564

Contents lists available at ScienceDirect

Engineering Science and Technology, an International Journal

journal homepage: www.elsevier.com/locate/jestch

Full Length Article

Optimal sizing of an integrated renewable energy system and effective utilization of surplus energy in electric vehicle charging

Vishal Saini *, S.K. Singal

Hydro and Renewable Energy Department, Indian Institute of Technology Roorkee, Roorkee 247667, Uttarakhand, India

ARTICLE INFO

Keywords:
Stand-alone integrated renewable energy system
Life cycle cost
Chimp optimization algorithm
Surplus energy
Electric vehicles
Integrated charging strategy

ABSTRACT

Renewable energy based power generation has proven to be a viable standalone option in areas where extending the grid is challenging. This study addresses this issue by assessing the possibility of an integrated renewable energy system (IRES) to electrify twelve villages in the Uttarakhand state of India. Four battery energy storage (BES) devices, namely Lead-Acid (LA), Sodium-Sulfur (NAS), Lithium-Ion (Li-Ion), and Nickel-Iron (Ni-Fe) are considered for storage in this study. Using the Chimp optimization algorithm (ChOA) on the MATLAB© platform, eight different configurations consisting of solar photovoltaic (SPV) array, a micro-hydropower (MHP) plant, and a biogas generator (BGG) are modeled and optimized. The study reveals that the optimal IRES configuration with the lowest cost and highest performance comprises 676 SPV panels (260 kWp), one MHP plant (25 kW), one BGG (40 kW), and 648 NAS batteries (778 kWh). This configuration has a total system life cycle cost (LCC) of INR 68.77 million and cost of energy (COE) of 16.77 INR/kWh at 0 % loss of power supply probability. The optimization problem was run 1–50 times and found that the proposed ChOA algorithm is more robust compared to others, displaying the lowest Best, Worst, and Mean values of LCC (across all eight configurations), convergence rapidity (26th iteration), and least computational time (3481 sec). However, GWO (seven configurations), MFO (34th iteration), and GA (4154 sec) stand very close to ChOA performance in terms of providing minimum LCCs, convergence rapidity, and computational time, respectively. Furthermore, surplus energy (SE) is effectively utilized by incorporating electric vehicles (EVs) as dump load in the system. The proposed integrated charging (IC) strategy outperforms other charging strategies by energizing 134 EVs, utilizing 99.59 % of SE, and reducing the total COE to 10.57 INR/kWh. Finally, the proposed IC strategy results in a net saving of 94,479.39 tons of greenhouse gas emissions. These findings support the feasibility of implementing a standalone IRES to electrify the study area and provide electricity to EVs.

1. Introduction

1.1. Motivation and incitement

Energy is one of the necessities in today's era for the welfare of the people [1]. However, a significant portion of the global population lacks access to basic energy services [2]. In developing countries, distributed renewable energy systems have emerged as a successful solution for meeting the electricity demand [3,4]. These systems, based on renewable energy sources, have proved particularly beneficial in remote rural communities where grid electrification is challenging and costly [5]. The idea of a renewable energy-based system, which is a microgrid encompassing various loads and generators in a confined region, is undergoing transformation because of increased effectiveness, minimal power loss during transmission, an economical transmission infrastructure, bolstered resilience, and heightened stability [6].

Nevertheless, renewable energy-based systems encounter various challenges, including the intermittent nature of renewable resources, the sizing of system components, system control, energy management, and power quality issues [22]. To address the intermittent nature of renewable energy (RE) sources, integrated renewable energy systems (IRESs) are often equipped with energy storage systems (ESSs) to ensure reliable matching of load demand [7,8]. In RE-based systems, batteries are considered prominently for energy storage purpose [9]. Batteries can augment solar and wind power, allowing for the optimization of total power output to maximize the use of renewable energy sources [10].

The conventional power system deals with variability in the form of random demand patterns. Whereas, RE-based power system introduces randomness in energy sources too. To address this increased variability

* Corresponding author.
E-mail address: vsaini@ah.iitr.ac.in (V. Saini).

https://doi.org/10.1016/j.jestch.2023.101564
Received 30 June 2023; Received in revised form 21 October 2023; Accepted 28 October 2023
Available online 16 November 2023

Nomenclature

Abbreviations

AC	Alternating current
ACs	Air conditioners
AEU	Annual energy utilization
BES	Battery energy storage
BGG	Biogas generator
BSC	Battery swapping charging
CC	Charge controller
CHP	Combined heat and power
CM	Chemicals
CO_2	Carbon dioxide
CH_4	Methane
ChOA	Chimp optimization algorithm
COE	Cost of energy
CRF	Capital recovery factor
CS	Cold storage
CSA	Cuckoo search algorithm
CT	Computational time
DBC	Dumb charging
DC	Direct current
DG	Diesel generator
DOD	Depth of discharge
EE	Excess energy
EMS	Energy management strategy
ESS	Energy storage system
EVs	Electric vehicles
FPA	Flower pollination algorithm
GA	Genetic algorithm
GHG	Greenhouse gas
GVs	Gasoline vehicles
GWO	Grey wolf optimization
HSA	Harmony search algorithm
IC	Integrated charging
ICC	Initial capital cost
IRES	Integrated renewable energy system
kWp	Peak-kilowatt
LA	Lead-Acid battery
LCC	Life cycle cost
Li-Ion	Lithium-Ion battery
LPSP	Loss of power supply probability
LPS	Loss of power supply
MA	Mayfly algorithm
MB	Membrane
MFO	Moth flame optimization
MHP	Micro-hydropower
NAS	Sodium-Sulfur battery
Ni-Fe	Nickel-Iron battery
N_2O	Nitrous oxide
OC	Operational cost
PC	Power converter
PHEVs	Plug-in hybrid EVs
PSO	Particle swarm optimization
PUF	Polyurethane foam
RE	Renewable energy
ROD	Reverse osmosis desalination
SC	Smart charging
SE	Surplus energy
SOC	State of charge
SPV	Solar photovoltaic
SSA	Salp swarm algorithm
WT	Wind turbine

Constant and variable parameters

A_{FC}	Annual fuel cost
A_{MC}	Annual maintenance cost
A_{RC}	Annual replacement cost
A_{temp}	Ambient temperature
C_{CWS}	Cost of civil work
C_{MS}	Cost of mechanical structure
C_{pw}	Present worth factor
$C_{ref,\ temp}$	SPV cell temperature under standard test conditions
CV_{BG}	Calorific value of biogas
CO_{2eq}	CO_2 equivalents
d	Journey distance
e_f	Emission factor
E_{BES}^{max}	Maximum energy storage limit of BES devices
E_{BES}^{min}	Minimum energy storage limit of BES devices
EE_{AC}	AC form of generated electrical energy
EE_{DC}	DC form of generated electrical energy
EE_{TD}	Electrical energy demanded
EE_{Gen}	Electrical energy generated
E_m	Annual GHG emission
F_{arr}	Arrival time of EVs
F_{dep}	Departure time of EVs
G	Solar radiation
G_{ref}	Solar radiation under standard test conditions
H_{BGG}	Daily operating hours of BGG
H_{CWD}	Hourly clean water demand
H_{net}	Net head of the MHP plant
N	Population size
P_L	Project lifetime
$P_{max,PC}$	Maximum power transmitted by the PC
Q_{BES}	Total count of BES devices
Q_{BES}^{max}	Maximum count of BES devices
Q_{SPV}	Total count of SPV panels
Q_{SPV}^{max}	Maximum count of SPV panels
Q_{BG}	Amount of biogas generated per day
Q_{CTD}	Quantity of cattle dung
$Q_{turbine}$	Design flow rate of the turbine
S_{BES}	Ampere-hour rating of BES devices
SOC_{BES}^{max}	Maximum SOC of BES devices
SOC_{BES}^{min}	Minimum SOC of BES devices
t_u	Usage time of component in years
T	Iterations in number
T_{coef}	Maximum power temperature coefficient of SPV panels
V_{BES}	Voltage rating of BES devices

Greek symbols

η_{BGG}	Efficiency of BGG
η_{CC}	Efficiency of CC
η_{MHP}	Efficiency of MHP plant
η_{PC}	Efficiency of PC
$\eta_{RT,BES}$	Round trip efficiency of BES devices
σ_{SDR}	Self-discharge rate of BES devices
σ_t	Standard deviation time of EVs
δ	Discount rate
δ_n	Nominal interest rate
μ	Inflation rate
μ_t	Mean time of EVs
ρ	Water density
Δt	Time step of one hour

Table 1
Summary of literature review.

Ref.	System components	Scenario	Approach	Evaluating criteria and constraints	Key results
[15]	PV/LA battery at 80 % DOD	Both grid-connected and stand-alone	GA	Total NPC, COE, constraints on the number of PV modules and batteries.	-NPC, COE of the grid-connected and stand-alone systems are found as $6,115, 0.183 $/kWh and $6,244, 0.196$/kWh, respectively.
[16]	PV/WT/DG/ LA and Li-Ion batteries	Stand-alone	PSO algorithm	Total NPC, LPSP, constraints on the capacity of PV panels, batteries, DG, converter and number of WTs.	-PV/Li-Ion battery with 100 % RF was found as optimal system with total NPC and COE of $23,427 and 0.23 $/kWh. -However, lower RF reduces energy consumption and CO_2 emission by 19 % and 57 %, respectively.
[17]	SPVG/WTG/ BMG/ BGG/LA battery	Stand-alone	Gradient descent algorithm and PSO algorithm	LCC, Energy index ratio (EIR), Expected energy not supplied (EENS), Excess energy, constraints on the number of SPV modules, WTGs, batteries, output power of BMG and BGG.	-SPV module of 0.25 kWp (Type-3), WTG of 1 kW (Type-1), and the LA battery of 360 Ah (Type-1) provided the least LCCs of 268242$, 252952$ and 305524$ at EIR of 85 %, 90 %, and 95 %, respectively.
[18]	SPV/WT/DG/ LA battery	Stand-alone	HOMER PRO software	NPC, COE, Life cycle emission, Renewable penetration (RP), Unmet load (UL), Duty factor, Human development index (HDI), Particulate matter, Job formation factor (JFF), Local transport-based employment (LTE).	-SPV/WT/DG/LA battery based optimal system provided the least NPC as 63,116$ and COE as 0.179$/kWh at 0 % unmet load. -The other social parameters viz: HDI, JFF and LTE was obtained as 0.6362, 0.0321 and 12.13, respectively.
[19]	solar/wind/DG/ PHS/LA battery at 70 % DOD	Stand-alone	SA algorithm	COE, Loss of load probability (LOLP), Payback time, Resource availability, Energy utilization ratio, RF, Environmental impact.	-Hybrid multi-criterion decision-making approach reveals that solar/wind/PHS/DG provided best results under four scenarios. -solar/wind/PHS provided best results under two Scenarios. -solar/wind/DG/LA battery provided best results under the no-preference scenario.
[20]	PV/wind/ biomass/ Zinc-Bromine battery/PHS	Both grid-connected and stand-alone	Generalized reduced gradient algorithm	Net present value (NPV), COE, RF, Demand supply fraction (DSF), Autonomy of the system.	-The best configuration was PV/wind/ biomass/Zinc-Bromine battery/PHS with COE, demand–supply fraction, and RF as 0.1626 $/kWh, 98.86 %, and 99.59 %, respectively.
[21]	PV panels/WTs/ battery bank/ DG/CHP/boiler/ thermal storage tank	Stand-alone	GA	Total NPV, Levelized Cost of Electricity (LCOE) and heat, total RP, RF, Excess ratio, and UL.	-This study showed that the steep price decline in renewable energy generators, particularly WTs and PV panels, significantly affects the optimal configuration.
[22]	PV/WT/DG/ Li-Ion battery	Both grid-connected and stand-alone	Pseudo-inspired gravitational search algorithm, and HOMER PRO software	ACS, LCOE, constraints on the maximum number of PV panels, WTs, maximum energy stored and supplied by the batteries, minimum and maximum DG generation, constraint on the power exchange between grid and system.	-Grid connected rural electrification is cheaper and more reliable (NPC of 320,395,303.04₦) than the stand-alone system (NPC of 416,355,120.39₦).
[23]	PV/WT/ Microturbine(MT) /FC/ nickel-metal hydride(Ni-MH) battery/ PHEV	Stand-alone	Hybrid whale optimization algorithm and pattern search (HWOAPS), GA, PSO, Pattern search (PS), and WOA.	Total OC, constraint on the power exchanged with the grid, limitations on the hourly power generation and demand, minimum and maximum power generated by the units, constraints on the charging and discharging rate of battery.	-Among all the algorithms HWOAPS provided the best results.-Scenario 1 (without PHEV) was cheaper (262.78 ¢ct) than scenario 2 (with PHEV) .-Scenario 2 provided the least charging cost (325.63 ¢ct) of PHEV under the SC plan.
[24]	PV/wind/DG/ plug-in EVs	Grid-connected	General algebra modeling system (GAMS)	Total OC, RE curtailment, emission benefits, limitations related to the DG operation, plug-in EV, DRP limits, AC-power flow equations, wind and PV power limits.	-The microgrid's DRP and electric vehicle synchronization reduce daily costs, DG generation, power purchase from the market, emission pollution, and RE curtailment by 9.97 %, 3.6 %, 3.8 %, 12.34 %, and 8.49 %, respectively.
[25]	WT/CHP/ hydrogen energy storage (HES) / plug-in EVs	Grid-connected	GAMS	Total OC, limitations on active and reactive power generation, WT generation, thermal and electrical power generation of a CHP unit, ramp up/down power throughput and minimum on/off time of generation units, HES limitations, DRP limits, gas network limitations.	-Integrating natural gas storage reduces pipeline congestion in the natural gas network, lowering operation costs. - HES, power to gas technology, and DRP increase system flexibility by reducing peak load. It reduces total operating costs.
[26]	Wind farm/PHEV	Grid-connected	GAMS	Energy cost, degradation cost of PHEV battery, emission curtailment, limitations on the PHEV fleet.	-Proposed system can influence locational marginal prices by 4.4 % and cut emissions by 40 %. -Ignoring battery degradation can increase operational costs dramatically.
[27]	PV/WT/battery at 80 % DOD/ EV	Grid-connected	Antlion optimization algorithm	COE, LPSP, RF, limitations on wind and SPV power, and on autonomy days.	-The proposed method achieves 0.0936 $/kWh, 0.1044 %, and 0.9940 % for COE, LPSP, and RF, respectively.

(*continued on next page*)

Table 1 (*continued*)

Ref.	System components	Scenario	Approach	Evaluating criteria and constraints	Key results
[28]	LUT energy system transition model	Grid-connected	MOSEK optimizer	ACS, LCOE, limitations on hourly heat and energy supply matches load demand.	-A fully integrated system can reduce the LCOE from 62 €/MWh in 2015 to 46 €/MWh in 2050, while heat stays at 30–35 €/MWh, resulting in an energy system cost of 40–45 €/MWh. -By 2050, 100 % renewable energy reduces CO_2eq emissions from these sectors to zero.
[29]	PV/WT/MT/FC/ Ni-MH battery/ PHEV	Grid-connected	Hybrid crow search-pattern search (HCS-PS) algorithm, GA, PSO, Crow search	Electricity price, limitations on hourly energy supply matches demand, on DG generation, limitations on energy supplied and absorbed by the grid and batteries.	-In the first and second scenario without PHEV, the HCS-PS algorithm provided best results of 262.7 €ct and 299.8 €ct, respectively. -In the first and second scenario with PHEV, the HCS-PS algorithm provided best results of 336.3 €ct and 326.6 €ct under smart charging method, respectively.
[30]	PV/WT/ Li-Ion battery/ EV charging stations	Stand-alone	HOMER PRO software, MOPSO, NSGA-II, NSGA-III, and MOEA/D	Total NPC, LPSP, WTs, PV panels and batteries	-PV/WT/battery system achieved the total NPC of $564,846, COE of 0.2521 $/kWh at 1.21 % LPSP. -Among the four algorithms, NSGA-II demonstrated the best overall performance.
[31]	WT/PV/BES/EVs	Grid-connected	GAMS	Total OC subjected to equality and inequality constraints	-In Case 4, the minimum total OC was $494,157.4 per day. This was 16.3 % lower than in Case 1, 4.2 % lower than in Case 2, and 1.3 % lower than in Case 3.

ACS = Annualized cost of the system, BMG = Biomass generator, DRP = Demand response program, MOEA/D = Multi-objective evolutionary algorithm based on decomposition, MOPSO = Multi-objective particle swarm optimization, NPC = Net present cost, NSGA = Non-dominated sorting genetic algorithm, WTG = Wind turbine generator, ₦ = Nigerian dollar.

stemming from RE resources, solving the problem requires the use of cutting-edge optimization tools capable of handling randomness [11]. It is noted that metaheuristic optimization algorithms have recently captured attention in the area of RE-based power system studies as they can efficiently tackle issues of randomness, and assist in operation control and energy management [22]. Moreover, they efficiently determine the quantities and dimensions of integrated system components while minimizing cost and addressing the common issue of converging to local minima, often encountered in traditional methods [12].

In these systems, excess energy generated during off-peak hours is used to charge the ESS. When the ESS is fully charged, any remaining excess energy (called surplus energy) is typically wasted in dump load that can be utilized in cooking, water heating, or baking [13]. Recently, electric vehicles (EVs) have played a crucial role in microgrid systems as emerging energy consumers, offering potential solutions to address system challenges [14]. Hence, EVs can be utilized as a promising consumer of surplus energy (SE) in future IRESs. As a result, the goal of this study is, firstly, to develop the optimal IRES model to electrify the chosen study area. Secondly, effective utilization of SE in standalone IRES for enhancing energy utilization and reducing the cost of energy by deploying EVs as a dump load.

1.2. Literature review

Several researchers have conducted studies on the optimal sizing problems of IRES from various perspectives. Hassan [15] used solar photovoltaic (PV)/lead acid (LA) battery-based system to meet the electricity needs of an Iraqi household in grid-connected and off-grid modes. Results reveal that in grid-connected and off-grid modes, 4,600 kWh/year and 1,468 kWh/year amount of SE is transferred to the grid and dump load, respectively. Mokhtara et al. [16] optimized wind turbine (WT)/PV/diesel generator (DG)/LA/lithium-ion (Li-Ion) battery-based off-grid system and found that the demand-side management at 100 % renewable fraction reduces SE transferred to dump load by 29 %.

Patel and Singal [17] conducted a study on an optimal system comprising 0.25 kWp of solar PV, 1 kW of WT, a biomass generator (BMG), a biogas generator (BGG), and a 360 Ah LA battery. They found that this system transmitted 14,124 kWh, 14,238 kWh, and 18,748 kWh amount of SE to the dump load at energy index ratio levels of 85 %, 90 %, and 95 %, respectively. Faizan et al. [18] found that the SPV/WT/DG/LA-based optimal system dumps 13,975 kWh/year amount of SE. Javed et al. [19] discovered that the optimal solar/wind/DG/LA/pump hydro storage (PHS) injected 25,450 kWh/year amount of SE to dump load.

Ghussain et al. [20] found that the optimal PV/wind/biomass and PV/wind/biomass/PHS/Zinc-Bromine battery-based system dumped 6,297 MWh and 4,811 MWh amount of SE to grid and PHS, respectively. Kahwash et al. [21] devised PV panels/WTs/battery bank/DG/CHP/boiler/thermal storage tank-based system and found that the total excess generation is more than 50 % with 15 % unutilized. Shukla and Momoh [22] discovered that the PV/DG/grid and PV/WT/DG/Li-Ion-based system generates 13,335 kWh/year and 11,818 kWh/year amount of SE in grid-connected and off-grid mode, respectively.

Recently integration of electric vehicles (EVs) in power systems has gained significant attention. In the present literature, several authors have incorporated EVs in their systems and analyzed their impacts on systems performance. Tao et al. [23] created a plug-in hybrid EV (PHEV)/PV/WT/Microturbine (MT)/Fuel cell (FC)/nickel-metal hydride (Ni-MH) battery system to reduce the system's operational cost (OC) by avoiding PHEV charging during peak demand. Guo et al. [24] investigated a system comprising PV/DG/plug-in EVs and demonstrated that integrating a demand response program with plug-in EVs lead to reductions in daily OC, DG generation, power purchases from the market, emission pollution, and renewable energy curtailment by 9.97 %, 3.6 %, 3.8 %, 12.34 %, and 8.49 %, respectively. Ibrahim et al. [25] integrated plug-in EVs into a system consisting of WT, CHP, and hydrogen energy storage, finding that the integration of plug-in EVs resulted in higher OC.

Zeynali et al. [26] investigated the integrated operation of a wind farm and PHEV fleets in a day-ahead wholesale market, taking into account the influence of battery degradation on OC under a smart charging scheme. Alsharif et al. [27] designed a microgrid comprising EVs, PV, WT, the grid, and batteries, aiming to minimize the COE while maximizing energy reliability and the renewable fraction. Bogdanov et al. [28] created a power, heat, transportation, and desalination energy system transition model to maintain the integrated energy system's total cost as low as possible.

Xiaoluan et al. [29] proposed a PHEV/grid/PV/WT/MT/FC/Ni-MH battery-based system and found that smart charging strategy reduces

Table 2
General information about the study area [42].

Property	Details
Country	India
State	Uttarakhand
District	Pithoragarh
Block	Munsyari
Name of villages	Milam, Bilju, Pachhu Gunth, Ganghar, Mapa, Burphu, Tola, Martoli, Lwa, Laspa, Khilach and Ralam.
Region	Hilly
Latitude and Longitude	30.36 N, 80.18 E
Number of households	335
Total population	1100
Population age group (0)–(6)	49
Literates	544
Language	Kumauni

Table 3
Daily seasonal energy demand in kWh.

Seasons	Minimum	Maximum	Average
Winter (Dec–Mar)	35	103	55
Summer (Apr–Jun)	8	101	45
Monsoon (Jul–Sep)	8	101	39
Post-monsoon (Oct–Nov)	8	76	28

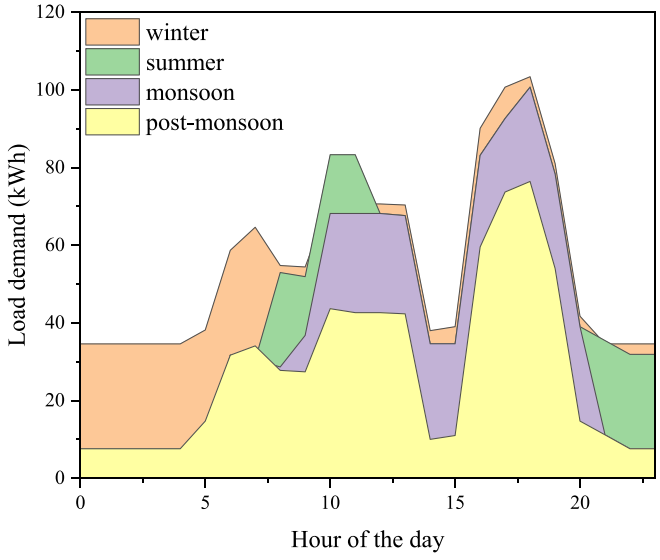

Fig. 1. Seasonal load demand curves.

PHEV charging cost significantly. Alshammari et al. [30] optimized hybrid EV charging systems for sustainability, considering technical and economic factors. Four different algorithms were deployed for multi-objective optimization, focusing on minimizing total NPC and reducing power supply interruptions. Reddy [31] proposed optimal scheduling for a microgrid, maximizing renewable energy use (wind and solar PV) while considering uncertainty. It minimized total operating cost (including grid exchange, renewables, storage, EVs, and demand response) using probability distribution functions and GAMS software.

The literature review is summarized in Table 1, which includes the main evaluating objectives, commonly used software and algorithms, and key findings from selected works in the literature.

The literature highlights several research gaps regarding the IRESs and the challenges associated with them. These points can be summarized as follows:

(i) The cost of storage, particularly batteries, is a significant concern in IRES due to the imbalance between renewable generation and demand. Surplus renewable generation often needs to be discarded to maintain system stability. The increased fraction of renewable energy and lower generation cost can further exacerbate this issue.
(ii) Many studies on IRES do not emphasize the utilization of SE effectively. This implies that there is potential to optimize the utilization of surplus renewable energy to enhance the overall efficiency and economic viability of IRES.
(iii) Several authors have considered EVs as part of the main load in IRES. Such integration of EVs increases the overall cost and size of the system. However, there is a lack of research on the charging of EVs in 100 % renewable energy-based stand-alone IRES, suggesting a gap in the current literature.

1.3. Contribution and paper organization

Based on the identified gaps in the literature, the novelty and significant contributions of this study can be outlined as follows:

(i) This study proposes the stand-alone IRES to meet the electricity demand of the selected villages in Munsyari Block of Uttarakhand state (India), using solar photovoltaic (SPV) array, micro-hydropower (MHP) plant, biogas generator (BGG), Lead-Acid (LA), Sodium-Sulfur (NAS), Lithium-Ion (Li-Ion) and Nickel-Iron (Ni-Fe).
(ii) Resilience, proficiency, and computational time performance of the proposed Chimp optimization algorithm (ChOA) [32] have been compared with other optimization algorithms such as Genetic algorithm (GA) [33], Particle swarm optimization (PSO) [34], Moth flame optimization (MFO) [35], Salp swarm algorithm (SSA) [36], Mayfly algorithm (MA) [37], Grey wolf optimization (GWO) [38], Cuckoo search algorithm (CSA) [39], Flower pollination algorithm (FPA) [40] and Harmony search algorithm (HSA) [41].
(iii) This study addresses the underutilization of surplus renewable energy in IRESs. It aims to develop an optimization strategy to effectively utilize the SE generated by renewable sources. Maximizing SE use improves the economic viability and efficiency of IRESs.
(iv) Unlike previous studies, this research investigates the charging of EVs in stand-alone IRES that solely rely on renewable energy sources. By exploring this aspect, it aims to provide insights into the feasibility, challenges, and potential benefits of integrating EV charging in 100 % renewable energy-based systems.

Overall, this study brings novel perspectives and significant contributions by addressing the gaps in existing literature, particularly in terms of SE utilization, EV integration in stand-alone IRES, cost and size optimization using a novel ChOA algorithm, and comprehensive performance analysis of the proposed ChOA algorithm with other optimization techniques.

To achieve the abovementioned objectives, details regarding the study area and load-resource assessment are provided in the subsequent Section 2. Afterward, Section 3 elaborates on the methodology adopted to carry out the study. Followed by Section 4, which presents the results and findings. Finally, Section 5 summarizes the paper and highlight the conclusions.

2. Identification of study area

The study area involves twelve un-electrified villages in the Munsyari Block of Uttarakhand, India. Munsyari Block is located in the Great Himalayas physiographic zone, at a high latitude, and low temperature. A heating season that can extend up to six months a year is brought on by

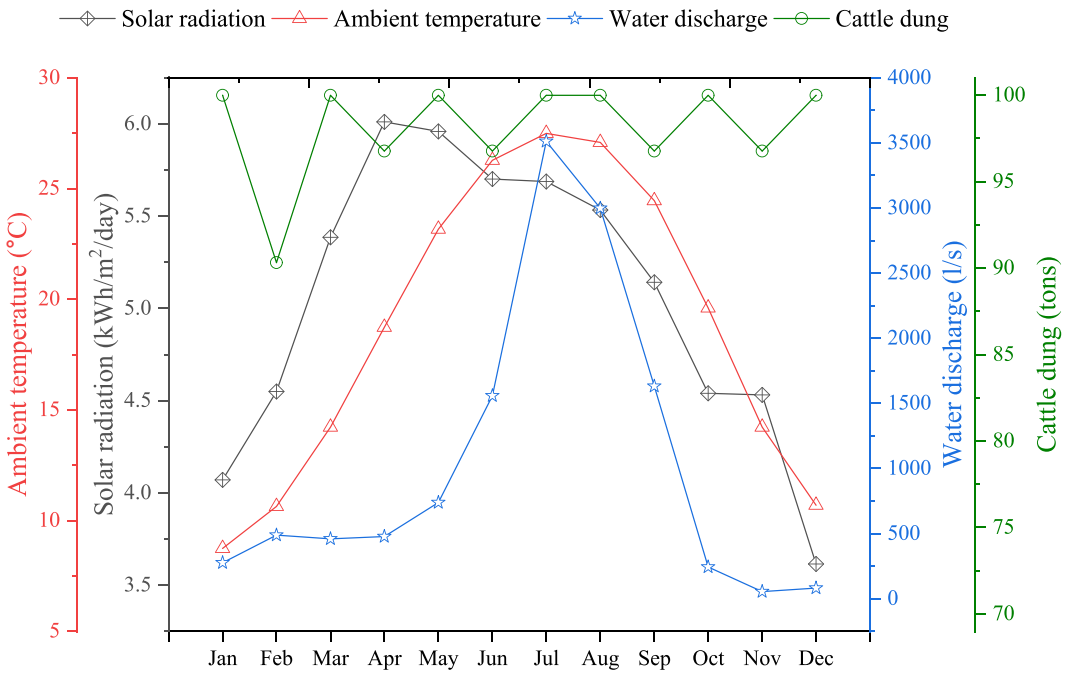

Fig. 2. Monthly profile of renewable resources.

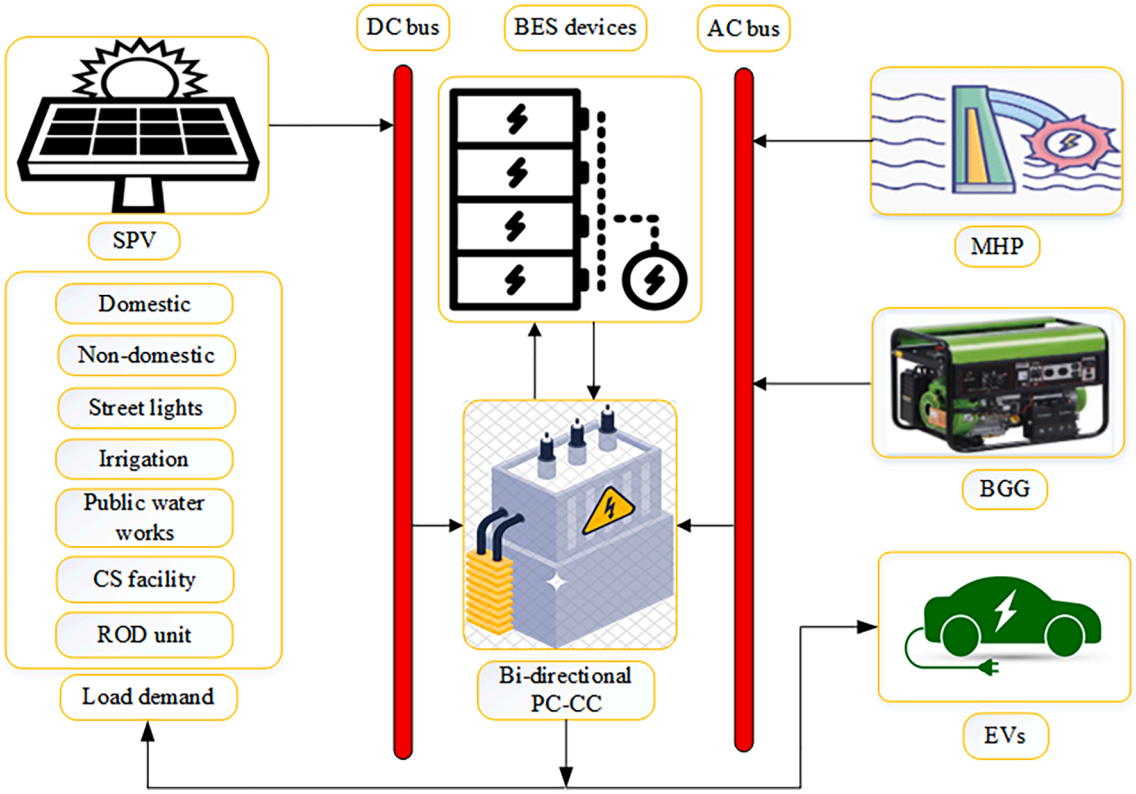

Fig. 3. Layout of the proposed integrated renewable energy system.

the long and chilly winters there. Table 2 contains general information about the study region.

2.1. Load-resource assessment of the study area

Daily load demand in the study area includes energy needs for various purposes such as domestic, non-domestic, street lights, irrigation, public water works, a cold storage (CS) facility, and a reverse osmosis desalination (ROD) unit. Table 3 presents the minimum, maximum, and average energy demand for different seasons. Additionally, Fig. 1 illustrates the seasonal load demand curves, showcasing the variations in load demand throughout the year.

During the site survey, it was observed that the study area has abundant solar radiation, water streams, and significant availability of

cattle dung for biomass. Solar radiation and ambient temperature data for a span of 20 years (1995–2015) were provided by the National Renewable Energy Laboratory (USA), as depicted in Fig. 2. The annual average solar radiation on an inclined plane recorded approx. 5 kWh/m^2/day, while the ambient temperature averaged 19 °C. In order to estimate the hydropower potential discharge, rainfall data spanning 20 years (1995–2015) were collected from the Indian Meteorological Department, Pune (India). Fig. 2 illustrates the monthly water discharge for the micro-hydropower (MHP) plant. Annual dependable water discharge for the MHP plant was estimated to be 232 L per second. In addition, the study area is home to a significant number of cattle, and their dung can be utilized to generate biogas and electricity [43]. Fig. 2 also demonstrates that the research region produces approximately 989 tons of dung per year, which is expected to yield around 42,705 cubic meters of biogas.

3. Methodology adopted

This section details power and economic modeling of all system components. Subsequently, this section explains the objective function and constraints of the study. Finally, it depicts the developed energy management strategy.

3.1. Power modeling of the integrated renewable energy system (IRES) components

The layout of the proposed IRES is shown in Fig. 3, which comprises SPV array, MHP plant, BGG, BES devices, Bi-directional power converter with a charge controller (PC-CC), load demands, and EVs as a dump load. The SPV array is connected to the DC bus, while the MHP plant and BGG are connected to the AC bus. The BES devices are connected to both the AC and DC bus through the bi-directional PC-CC. This allows them to store and supply power as needed. Similarly, the EVs are also connected to both the buses through the bi-directional PC-CC, enabling them to consume the SE generated on an hourly basis.

3.1.1. Solar photovoltaic (SPV) array

The SPV array mainly comprises several SPV panels that transform solar energy into electricity. Based on hourly solar radiation (G (t)) and ambient temperature (A_{temp} (t)), the power delivered by the SPV array (P_{SPV} (t)) can be calculated as [16]:

$$P_{SPV}(t) = SPV_{rated}\left(\frac{G(t)}{G_{ref}}\right)\{1+([A_{temp}(t)+0.0256*G(t)] - C_{ref,temp})T_{coef}\}Q_{SPV} \quad (1)$$

where, SPV_{rated} is the SPV panel's rated output power. G_{ref} and $C_{ref,\ temp}$ are solar radiation and SPV cell temperature under standard conditions, respectively. T_{coef} is the maximum power temperature coefficient (0.0037/°C) and Q_{SPV} is the total count of SPV panels.

3.1.2. Micro-hydropower (MHP) plant

The assessment of hydropower potential in this study is conducted using the soil conservation service-curve number method, as described in reference [44]. This method is utilized to estimate the monthly discharge of direct run-off stream, as depicted in Fig. 2. Hourly power output of the MHP plant (P_{MHP} (t)) in kW is evaluated by using Eq. (2) as [44]:

$$P_{MHP}(t) = \frac{9.81 \times \rho \times Q_{turbine} \times H_{net} \times \eta_{MHP}}{1000} \quad (2)$$

where, ρ is the water density (1000 kg/m^3), $Q_{turbine}$ is the design flow rate of the hydro turbine, H_{net} is the net head (18.25 m), and η_{MHP} is the overall efficiency of the MHP plant (60 %). Based on the available head and discharge, the MHP plant of 25 kW capacity has been proposed in the study area.

3.1.3. Biogas generator (BGG)

The total power generated by the BGG (P_{BGG} (t)) in kW on daily basis is expressed by Eq. (3) as [17]:

$$P_{BGG}(t) = \frac{Q_{BG} \times CV_{BG} \times \eta_{BGG}}{860 \times H_{BGG}} \quad (3)$$

where, Q_{BG} is the amount of biogas generated per day (117 m^3), CV_{BG} is the calorific value of biogas (4700 kcal/m^3), η_{BGG} is the efficiency of BGG (25 %), and H_{BGG} is the daily operating hours of BGG (4 h from 4p. m. to 8p.m.).

3.1.4. Battery energy storage (BES) devices

Excess energy stored by the BES devices when hourly energy generation exceeds load demand is illustrated by Eq. (4). Similarly, the required deficit load supplied by the BES devices when hourly load demand exceeds energy generation is illustrated by Eq. (5). The available capacity of BES devices at time t can be stated as [45]:

$$E_{BES}(t) = \left[(1-\sigma_{SDR}) \times E_{BES}(t-1) + \left(\frac{EE_{Gen}(t) - EE_{TD}(t)}{\eta_{PC}}\right) \times \eta_{CC} \times \eta_{RT,BES}\right] Q_{BES} \quad (4)$$

$$E_{BES}(t) = \left[(1-\sigma_{SDR}) \times E_{BES}(t-1) - \left(\frac{EE_{TD}(t)}{\eta_{PC}} - EE_{Gen}(t)\right) \Big/ \eta_{RT,BES}\right] Q_{BES} \quad (5)$$

$$EE_{Gen}(t) = (EE_{DC} + EE_{AC}) \times \eta_{PC} \quad (6)$$

$$EE_{DC}(t) = P_{SPV}(t) \times \Delta t \quad (7)$$

$$EE_{AC}(t) = (P_{MHP}(t) + P_{BGG}(t)) \times \Delta t \quad (8)$$

where, E_{BES} (t) and E_{BES} (t-1) are the states of energy of BES devices at the time 't' and 't-1', respectively. σ_{SDR} is the hourly self-discharge rate of BES devices. EE_{Gen} (t) and EE_{TD} (t) are the total electrical energy generated and demanded at any time 't', respectively. η_{PC} is the efficiency of power converter (PC), η_{CC} is the efficiency of charge controller (CC), $\eta_{RT,\ BES}$ is the round-trip efficiency of the BES devices, and Q_{BES} is the total count of BES devices. EE_{DC} and EE_{AC} are the generated direct current (DC) and alternating current (AC) forms of electrical energy, respectively. Δt is the time step of one hour.

3.1.5. Bi-directional power converter with a charge controller (PC-CC) system

The bi-directional power converter (PC) in the system serves two purposes: converting AC to DC in rectifier mode and DC to AC in inverter mode. This allows for the utilization of both AC and DC electrical energy in the system. In IRES, charge controllers (CC) play a pivotal role in safeguarding BES devices against potential harm caused by excessive charging and discharging. It is achieved by regulating the flow of current to and from the BES devices, ensuring their longevity and optimal performance. The power rating of bi-directional PC-CC ($P_{PC\text{-}CC}$) is calculated by Eq. (9) as:

$$P_{PC-CC} = P_{max,PC} \times 1.1 \quad (9)$$

where, $P_{max,PC}$ is the maximum power transmitted by the PC and the multiplication factor of 1.1 shows the 10 % overloading capacity of the PC [17].

Additionally, one ROD unit and one CS facility are proposed in this study. They require 2 kWh and 4.22 kWh, respectively, on a daily basis.

3.1.6. Integration of electric vehicles (EVs) as dump load with the IRES

Electric vehicle charging demand is determined by analyzing the

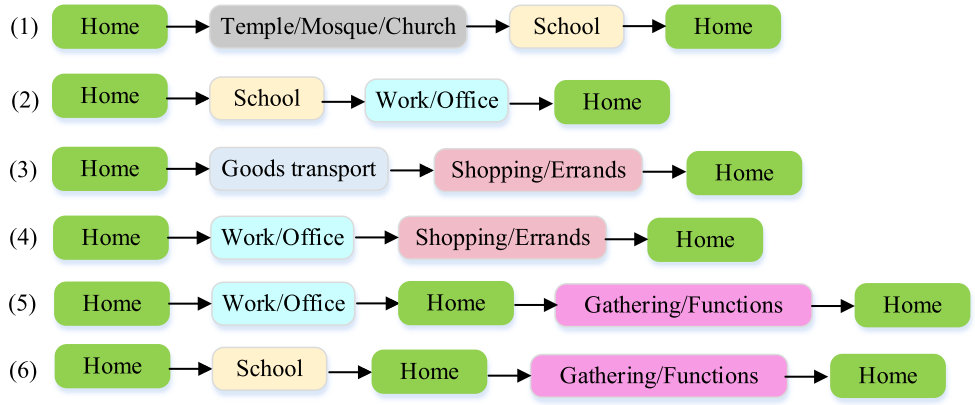

Fig. 4. Typical trip chains prepared from daily activities.

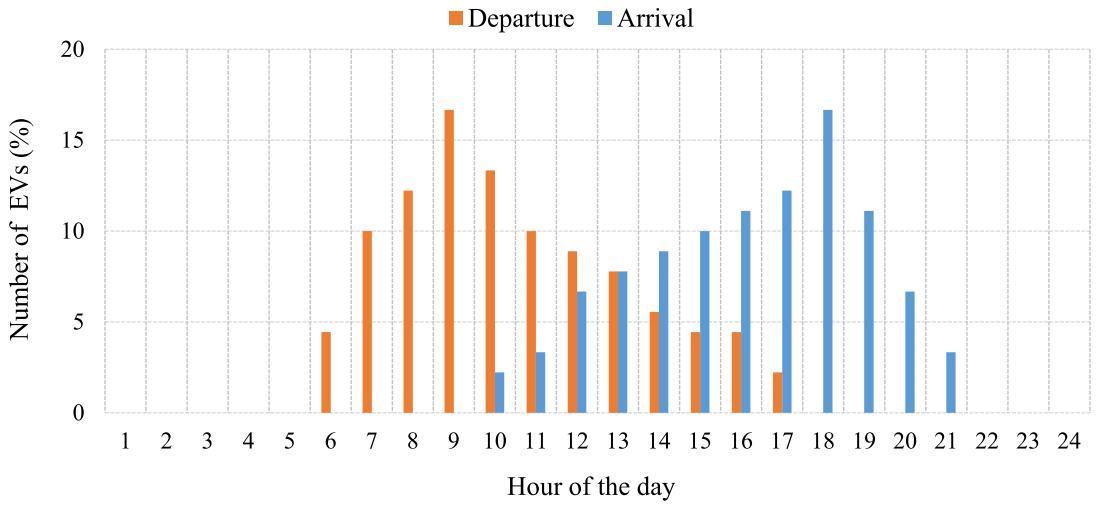

Fig. 5. Hourly departure and arrival time of EVs.

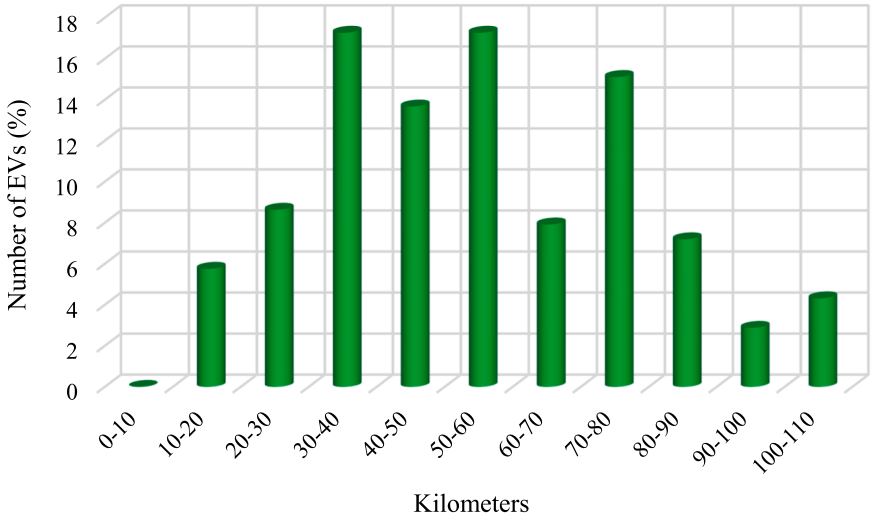

Fig. 6. Daily distance covered by EVs.

daily travel profiles. Data on daily driving patterns were obtained from the Uttarakhand Transport Corporation and residents in the study area. The dynamic travel patterns were captured using the trip chain model, which is based on daily driving patterns [46]. Fig. 4 illustrates six representative trip chains that reflect daily activities. It is observed that most EVs are charged during the night and early morning hours when they are parked. The hourly departure and arrival timing of EVs are shown in Fig. 5, while Fig. 6 displays the daily travel distance of EVs.

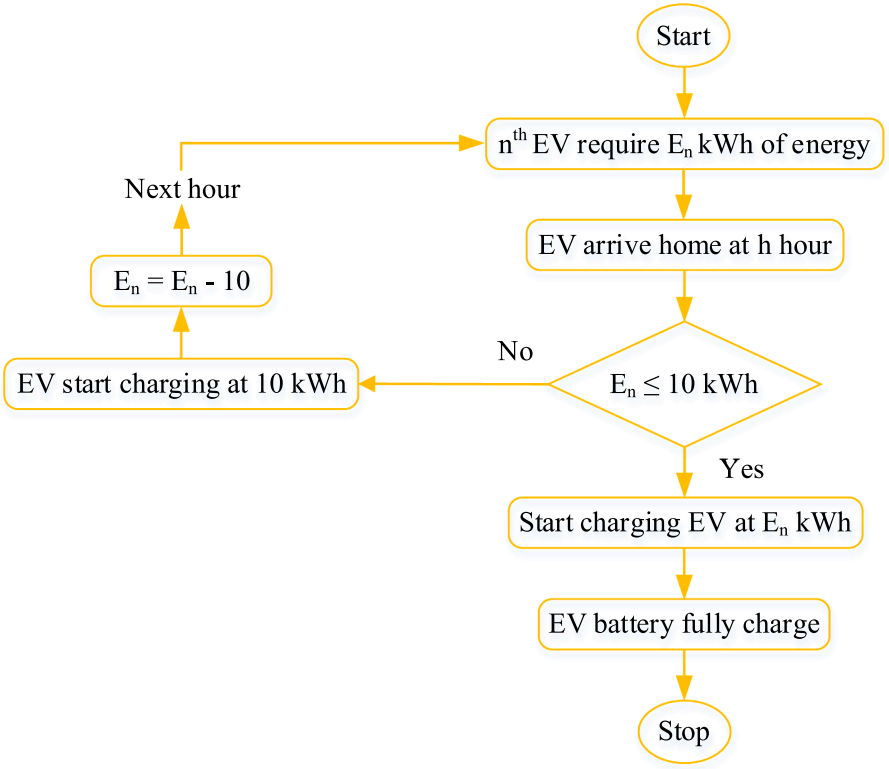

Fig. 7. Charging strategy for EVs.

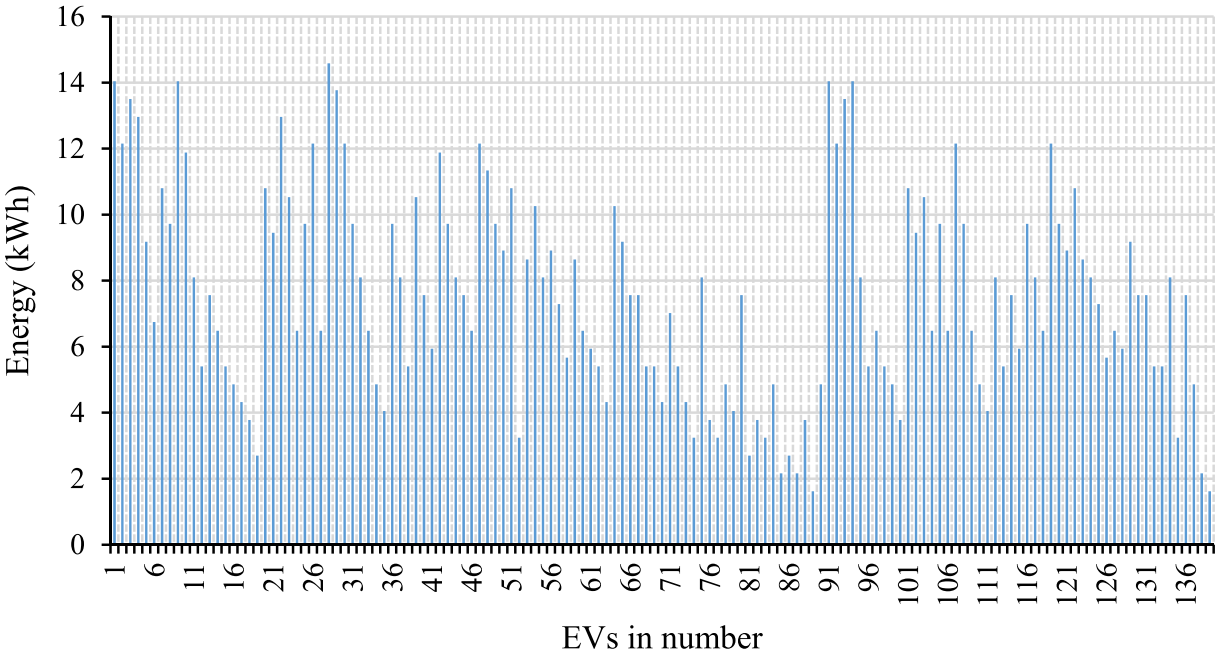

Fig. 8. The energy required by EVs for daily distance travel.

For the various factors that contribute to the unpredictability of EVs charging demand, such as driver behavior, travel patterns, and charging infrastructure availability, a normal distribution function is employed. To account for the stochastic behavior of EV drivers, the probability distribution function of the departure (F_{dep} (t)) and arrival (F_{arr} (t)) time of EV drivers are considered which is a normal distribution that can be expressed by Eqs. (10) and (11), respectively as [47]:

$$F_{dep}(t) = \frac{1}{\sigma_t\sqrt{2\pi}} e^{-(t-\mu_t)/2\sigma_t^2},\ 0 < t < 24 \tag{10}$$

where, $\mu_t = 10.5$, $\sigma_t = 3.45$

$$F_{arr}(t) = \frac{1}{\sigma_t\sqrt{2\pi}} e^{-(t-\mu_t)/2\sigma_t^2},\ 0 < t < 24 \tag{11}$$

Table 4
CO_2 emission from the IRES.

Emission source	GHG emission (E_m in tons)	Emission factor (e_f in $kgCO_2$/kWh)
Grid	$E_{m,Grid} = \sum_{t=1}^{8760} EE_{TD}(t)*e_{f,Grid}$	0.79 [53]
SPV	$E_{m,SPV} = \sum_{t=1}^{8760} P_{SPV}(t)*e_{f,SPV}$	0.046 [19]
MHP	$E_{m,MHP} = \sum_{t=1}^{8760} P_{MHP}(t)*e_{f,MHP}$	0.009 [54]
BGG	$E_{m,BGG} = \sum_{t=1}^{8760} P_{BGG}(t)*e_{f,BGG}$	0.099 [54]

where, $\mu_t = 14.5$, $\sigma_t = 3.6$

To account for the stochastic travel pattern of EVs, the probability distribution function of the daily distance (F_d (d)) covered by EVs is considered and is evaluated by Eq. (12) as [47]:

$$F_d(d) = \frac{1}{d\sigma_t\sqrt{2\pi}} e^{-(\ln(d)-\mu_t)/2\sigma_t^2},\ d > 0 \tag{12}$$

where, d is the journey distance, μ_t is the mean of $\ln(d)$ (55.62), and σ_t is the standard deviation (24.16).

The following assumptions are taken into account in the EV charging analysis:

(i) The probability of charging infrastructure availability at home is 100 %.
(ii) This study takes into consideration the capital cost per kilowatt of all standby EV batteries, as outlined later in Table 6.
(iii) For simplification, it is also assumed that the standby EV batteries have a lifespan of 20 years.
(iv) To ensure that future EVs are efficient, this study assumes an EV energy consumption rate of 0.135 kWh/km [48].

In this study, EVs are equipped with a 16.2 kWh Li-Ion battery and 10 kWh charger capacity. Fig. 7 presents the developed EV charging strategy, based on the hourly energy required by the EVs as shown in Fig. 8. Each EV is associated with a specific arrival time, and charging begins when the EV arrives at home [49]. For instance, if the energy consumption of an EV is below 10 kWh upon arrival, charging proceeds at the current energy level until the battery is fully charged. However, if the energy consumption is higher, charging occurs at a rate of 10 kWh.

3.1.7. Avoided greenhouse gas (GHG) emission

Avoided GHG emission is an important environmental indicator that represents the reduction in equivalent carbon dioxide (CO_2) emissions achieved by implementing IRES and EVs, compared to the emissions that would have been produced if the conventional grid and gasoline vehicles (GVs) were used instead. The calculation of avoided GHG emissions in this study is expressed by the following formula [50]:

$$GHG = (GHG_{Grid} + GHG_{GVs}) - (GHG_{SPV} + GHG_{MHP} + GHG_{BGG} + GHG_{EVs}) \tag{13}$$

In this study, the emission of CO_2 from EVs is assumed to be zero, while from GVs is considered to be 0.1135 $kgCO_2$ per kilometer [51], Table 4presents the equations used to estimate the CO_2 emissions from the IRES.

To compare the emissions of different GHGs, they are expressed in terms of CO_2 equivalents (CO2eq). CO_2 is used as a baseline with a global warming potential of one, while other GHGs specified in the Kyoto Protocol have higher global warming potentials than CO_2 [52]. This allows for standardized measurement of emissions and their impact on global warming.

3.2. Economic analysis modeling of the IRES

The life cycle cost (LCC) of the system includes initial capital cost (ICC), cost of mechanical structure (C_{MS}) of SPV panels, cost of civil works (C_{CWS}), annual maintenance cost (A_{MC}), annual replacements cost (A_{RC}), and annual fuel cost (A_{FC}).

The following assumptions are taken into account in the economic analysis:

(i) C_{CWS} of all the IRES components viz: SPV panels, MHP plant, BGG, BES devices, PC-CC, ROD unit, and CS facility are considered as 20 % [17], 40 % [55], 5 % [17], 3 % [17], 3 % [17], 3 % [56], and 108 % [57] of their initial capital cost, respectively.
(ii) A_{MC} of IRES components viz: SPV panels, BGG, PC-CC, and CS facility are considered as 2.5 % [17], 2.5 % [17], 2.5 % [17], and 2 % [57] of their initial capital cost, respectively. Whereas, A_{MC} of the MHP plant and ROD unit are taken as 7500 INR/kW [33] and 15 INR/m^3 [56], respectively.
(iii) A_{RC} of all the IRES components viz: BGG, BES devices, PC-CC, MB (membrane), CM (chemicals), ACs, and PUF insulation material are considered as 70 % [17], 100 % [17], 100 % [17], 100 % [56], 100 % [56], 100 % [57], and 100 % [57] of their initial capital cost, respectively.

The overall LCC of the IRES is estimated by Eq. (14) as [17]:

$$LCC = \sum ICC + \sum C_{MS} + \sum (C_{CWS} + A_{MC} + A_{RC} + A_{FC}).C_{PW} \tag{14}$$

where, C_{pw} is a present worth factor which includes the change in the value of money over time. It is calculated as follows [17]:

$$C_{PW} = \sum_{i=1}^{t_u} \frac{(1+\mu)^{i-1}}{(1+\delta)^i} \tag{15}$$

$$\delta = \frac{\delta_n - \mu}{1+\mu} \tag{16}$$

where, δ, δ_n, μ, and t_u represent the discount rate, nominal interest rate, inflation rate, and usage time of component in years, respectively. Finally, the cost of energy (COE) is evaluated as:

$$COE\left(\frac{INR}{kWh}\right) = \left(\frac{LCC}{\sum_{t=1}^{8760} EE_{TD}(t)}\right) \times CRF \tag{17}$$

where, CRF is the capital recovery factor and is expressed as:

$$CRF = \frac{\delta(1+\delta)^{P_L}}{(1+\delta)^{P_L} - 1} \tag{18}$$

where, P_L is the project lifetime of 20 years.

3.3. Objective function and constraints

The life cycle cost as an objective function and the constraints that were taken into account are explained below.

3.3.1. Life cycle cost (LCC)

The objective function of this study is to minimize the LCC by considering constraints. The objective function is written as:

$$\text{Minimize} LCC(Q_{SPV}, Q_{BES}) = \sum_{m=SPV,MHP,BGG,BES,PC-CC,ROD,CS}^{min} (LCC)_m \tag{19}$$

3.3.2. Energy balance constraints

The equality constraint in the IRES ensures the equilibrium between instantaneous energy generation and load demand. This constraint can be articulated as follows:

$$(P_{BGG}(t) + P_{MHP}(t) + P_{SPV}(t)) \times \Delta t \pm E_{BES}(t) = EE_{TD}(t) + E_n^t \tag{20}$$

where, E_n^t is the SE consumed by the n^{th} EV at hour 't'.

Table 5
Techno-economic parameter values.

Parameter	Value	Parameter	Value
Nominal interest rate (%)	13	ICC of ROD unit (INR)	156,600
Annual inflation rate (%)	5	ICC of WST (INR)	76,800
Rated power of SPV panel (W_P)	385	ICC of MB (INR)	18
ICC of SPV panel (INR)	9,600	ICC of CM (INR)	18
Lifetime of SPV panel (years)	20	No. of MB replacement/year	2
MS cost of each SPV panel (INR)	3,075	Rated power of air conditioners (kW)	4.22
Lifetime of MS of SPV panel (years)	20	ICC of air conditioners (INR)	135,000
MHP plant capacity (kW)	25	Lifetime of air conditioners (years)	10
ICC of MHP plant (INR/kW)	97,500	ICC of PUF insulation (INR)	52,500
Lifetime of MHP plant (years)	20	ICC of humidifier (INR)	18,750
Rated power of BGG (kW)	40	ICC of sensors (INR)	2,250
ICC of BGG (INR)	559,050	Rated power of PC-CC (kW)	114
Lifetime of BGG (hours)	20,000	ICC of converter (INR)	92,340
Dung consumed by BGG (tons/year)	889	Lifetime of converter (years)	10
Cost of cattle dung (INR/ton)	750	Efficiency of converter (%)	95

3.3.3. Upper and lower bound constraints

This study considers the total count of SPV panels (Q_{SPV}) and BES devices (Q_{BES}) as decision variables, as expressed by Eqs. (20)-(21):

$$0 \le Q_{SPV} \le Q_{SPV}^{max} \tag{21}$$

$$0 \le Q_{BES} \le Q_{BES}^{max} \tag{22}$$

3.3.4. Energy storage limit on the BES devices

The following expression limits the amount of energy stored in the BES devices at any time 't' given by Eq. (23),

$$E_{BES}^{min} \le E_{BES}(t) \le E_{BES}^{max} \tag{23}$$

The following are the maximum and minimum energy storage limits for BES devices:

$$E_{BES}^{max} = \left(\frac{Q_{BES} \times V_{BES} \times S_{BES}}{1000}\right) \times SOC_{BES}^{max} \tag{24}$$

$$E_{BES}^{min} = \left(\frac{Q_{BES} \times V_{BES} \times S_{BES}}{1000}\right) \times SOC_{BES}^{min} \tag{25}$$

where, V_{BES} is the rated voltage and S_{BES} is the rated ampere-hour (Ah) capacity of each BES device.

The minimum and the maximum state of charge of BES devices are as follows:

$$SOC_{BES}^{min} = 1 - DOD \tag{26}$$

$$SOC_{BES}^{max} = SOC_{BES}^{min} + DOD \tag{27}$$

where, SOC is the state of charge and DOD is the depth of discharge.

3.3.5. Power reliability constraint

The loss of power supply probability (LPSP) occurs when IRES is not able to meet the energy demand. This study evaluates hourly power losses (LPS(t)) using hourly generated electricity, hourly load demand, and BES devices energy level at any time (t):

$$LPS(t) = \left(\frac{EE_{TD}(t)}{\eta_{PC}}\right) - EE_{Gen}(t)\left[(1-\sigma_{SDR}) \times E_{BES}(t-1) - E_{BES}^{min}\right] \times \eta_{RT,BES} \tag{28}$$

The LPSP is expressed as follows:

$$LPSP = \frac{\sum_{t=1}^{8760} LPS(t)}{\sum_{t=1}^{8760} EE_{TD}(t)} \tag{29}$$

3.4. Energy management strategy (EMS)

EMS ensures efficient operation of the IRES by allocating energy units to meet system demand while minimizing LCC and adhering to reliability constraints. It optimizes the utilization of energy sources (BGG, MHP, and SPV) based on availability, cost, and reliability considerations. The EMS is explained as follows:

(i) If the IRES generates energy equal to the load demand, it is injected into the main load using the bi-directional PC-CC.
(ii) If the total energy generated by the IRES is less than the load demand, then BES devices supply the load demand. If the BES devices are unable to fully supply the load demand, a portion of the load is interrupted, resulting in the LPSP as the reliability index.
(iii) If the total energy generated by the IRES is greater than the load demand, the excess energy is delivered to the BES devices. If the injected energy to the BES devices exceeds their rated capacity or the BES devices are full, the remaining excess energy (called surplus energy) is used to charge the EVs.

4. Results and discussion

This analysis involves a thorough examination of the best possible configuration and scheduling strategy for renewables BGG, MHP, and SPV with various BES devices, including, LA, Li-Ion, NAS, and Ni-Fe. To find the optimal solution, numerous optimization algorithms are employed, such as ChOA, GA, PSO, MFO, SSA, MA, GWO, CSA, FPA, and HSA, which are implemented within the optimization model to identify the most favorable configuration. The optimal configuration is determined based on the concept of the system's least LCC. To gauge the performance of these algorithms, a model is established to assess criteria like resilience, proficiency, and computational time. The primary objective of this methodology is to pinpoint the most appropriate BES device and algorithm for achieving optimal results in a system driven by BGG, MHP plant, and SPV panels. Lastly, the approach is employed to charge EVs using the SE generated by the IRES, following different EV charging strategies.

The total count of SPV panels (Q_{SPV}) and BES devices (Q_{BES}) are considered decision variables and optimized in this study. Whereas, MHP plant, BGG, and converter system capacities are considered fixed variables. Thus, based on the provided upper and lower limit values of the optimized variable in search space, the optimization algorithm will give the optimum value of that particular component. The BGG generates electricity at its rated capacity throughout the project lifetime. The MHP plant, on the other hand, is expected to generate electricity at its rated capacity for more than 75 % of the year.

4.1. Identification of optimal IRES configuration

This study examines different configurations of the IRES involving BGG, MHP plant, SPV panels, and BES devices with varying depths of discharge (DOD). Four types of BES devices (LA battery, NAS battery, Ni-Fe battery, and Li-Ion battery) are considered for optimization. Earlier ChOA algorithm has been used to address various issues such as breast cancer detection, optimal location of DGs, underwater acoustical dataset, real-time COVID-19 diagnosis from x-ray images, diagnosis of Parkinson's disease and cleft lip and palate, except optimal sizing of the IRESs. Therefore, in this study, the ChOA algorithm is implemented in MATLAB© to determine the optimal IRES configuration. A total of eight configurations are simulated and optimized at 0 % LPSP level. The

Table 6
Techno-economic specification of BES devices.

Battery	Lead-Acid (LA)	Lithium-Ion (Li-Ion)	Sodium-Sulfur (NAS)	Nickel-Iron (Ni-Fe)
Battery capacity (Ah)	490	300	600	1000
Voltage rating (V)	6	12.8	2	1.2
Round-trip efficiency (%)	85	92	90	80
Total lifetime (years)	3 at 70 % DOD 2.5 at 80 % DOD	9 at 70 % DOD 7.5 at 80 % DOD	20 at 70 % DOD 15 at 80 % DOD	30 at 70 % DOD 30 at 80 % DOD
Self-discharge rate (%)	0.30	0.20	0.20	1
ICC (INR)	30,750	248,775	45,000	79,275
A_{MC} (INR)	2.5 % of ICC	Nil	2 % of ICC	2 % of ICC

Table 7
Parameter settings of algorithms.

Algorithm	Parameters		
GA	N = 100	T = 100	$\mu = 0.1$, CR = 0.9
PSO	N = 100	T = 100	$W_{max} = 0.9$, $W_{min} = 0.2$, c_1 and $c_2 = 2$
MFO	N = 100	T = 100	a = -1 to −2, b = 1
SSA	N = 100	T = 100	c_1 = rand (0,1), c_2 = rand (0,1), c_3 = rand (0,1)
ChOA	N = 100	T = 100	m = chaotic, a = 2.5 to 0, f = -1 to 1, r_1 and r_2 = rand (0,1)
MA	N = 100	T = 100	g = 0.8, $a_1 = 1$, $a_2 = 1.5$, $\beta = 2$, d = 5, $f_1 = 1$, CR = 0.9
CSA	N = 100	T = 100	pa = 0.25, $\lambda = 1.5$, $\alpha = 0.01$ to 0.1
GWO	N = 100	T = 100	a = 2 to 0, A = (-2a, 2a), C = rand (0,2)
FPA	N = 100	T = 100	p = 0 to 1, $\gamma = 10^{-4}$ to 1, $\lambda = 1.5$
HSA	N = 100	T = 100	p = 0 to 1, m = 0.9, $n_b = 0.3$

simulations are performed on a computer with an Intel (R) Core (TM) i5-3470 CPU and 8 GB of RAM. The values of techno-economic parameters of all materials used are shown in Tables 5 and 6. Further, Table 7 displays the parameter settings for the algorithms used.

4.1.1. Performance analysis of LA battery configured IRES configuration

From Table 8, it is observed that the IRES configuration with LA battery (BGG/MHP/SPV) at 80 % DOD yield the best results. The corresponding LCC is INR 82.29 million, and the COE is 20.07 INR/kWh. This configuration exhibits a reduction of approximately 0.73 % compared to the BGG/MHP/SPV/LA at 70 % DOD configuration. The optimal values for Q_{SPV} and Q_{BES} are found 743 and 244, respectively.

4.1.2. Performance analysis of Li-Ion battery configured IRES configuration

According to the results presented in Table 8, the Li-Ion battery performs best with the BGG/MHP/SPV configuration at 80 % DOD. The corresponding LCC and COE are obtained as INR 137.69 million and 33.59 INR/kWh, which are approximately 8.87 % lower than the BGG/MHP/SPV/Li-Ion at 70 % DOD configuration. At 80 % DOD, the Q_{SPV} and Q_{BES} corresponding to the BGG/MHP/SPV/Li-Ion are found 654 and 173, respectively.

4.1.3. Performance analysis of NAS battery configured IRES configuration

Based on the findings presented in Table 8, the NAS battery demonstrates the most favorable outcome when combined with the BGG/MHP/SPV configuration at 70 % DOD. The associated LCC is INR 68.77 million, and the COE is 16.77 INR/kWh. These values indicate an approximate 17.09 % decrease compared to the BGG/MHP/SPV/NAS at 80 % DOD configuration. The optimal values for Q_{SPV} and Q_{BES} are 676 and 648, respectively.

4.1.4. Performance analysis of Ni-Fe battery configured IRES configuration

The optimization results given in Table 8 show that the Ni-Fe battery performs best with BGG/MHP/SPV at 80 % DOD configuration, producing LCC and COE of INR 103.575 million and 25.26 INR/kWh, respectively, which are approximately 12.08 % lower than the BGG/MHP/SPV/Ni-Fe at 70 % DOD configuration. The Q_{SPV} and Q_{BES} values for BGG/MHP/SPV/Ni-Fe at 80 % DOD configuration are found 836 and 671, respectively.

The findings from subsection 4.1 lead to the following conclusions: (i) Among all the batteries considered, the BGG/MHP/SPV configuration combined with the NAS battery at 70 % DOD yields the best results. (ii) The NAS battery, LA battery, Ni-Fe battery, and Li-Ion battery exhibit the lowest LCCs and COEs in that order. Based on these results, it is recommended to implement the BGG/MHP/SPV/NAS configuration at 70 % DOD for the electrification of the study area as it offers the most favorable outcomes.

4.2. Performance analysis of the proposed ChOA algorithm

In this study, the performance of the proposed ChOA algorithm is compared with other optimization algorithms, including Genetic algorithm (GA), Particle swarm optimization (PSO), Moth flame optimization (MFO), Salp swarm algorithm (SSA), Mayfly algorithm (MA), Grey wolf optimization (GWO), Cuckoo search algorithm (CSA), Flower pollination algorithm (FPA) and Harmony search algorithm (HSA). The comparison is based on several factors, namely Best, Worst, and Mean values of LCC, convergence rapidity, and computational time (CT).

Table 8 shows LCC results for all optimized configurations using different algorithms. The Best, Worst, and Mean LCC values show how well each algorithm finds the optimal solution. Each algorithm's CT for one run simulation is shown in seconds (sec). The average CT was estimated from 50 run simulations for all configurations.

Comparing the results shows each algorithm's resilience and ability to solve the IRES configuration problem optimally. The CT shows how fast algorithms solve problems. These comparative results help assess the ChOA algorithm's solution quality and computational efficiency advantages over other optimization algorithms.

4.2.1. Algorithm ranking based on best, worst, and mean values of LCC

The rankings of the ten algorithms are detailed below to get the overall Best, Worst, and Mean values of LCCs:

The GA and HSA both ranked seventh by providing the lowest Best, Worst, and Mean values of LCC in two, zero, and zero configurations, respectively, out of the eight configurations. The CSA is ranked sixth because it only produced the lowest Best, Worst, and Mean values of LCC in four, zero, and zero configurations. The PSO and FPA both ranked fifth because they only produced the lowest Best, Worst, and Mean values of LCC in five, two, and two configurations. The MA is ranked fourth because it only produced the lowest Best, Worst, and Mean values of LCC in five, three, and three configurations. The MFO and SSA are ranked third because they produced the lowest Best, Worst, and Mean values of LCC in six, five, and five configurations. The GWO is ranked second because it produced the lowest Best, Worst, and Mean values of LCC in seven, six, and six configurations. Finally, the ChOA is ranked first because it produced the lowest Best, Worst, and Mean values of LCC across all eight configurations.

These rankings show how well each algorithm finds optimal LCC values for different IRES configurations. The ChOA algorithm produces the better Best, Worst, and Mean LCC results across all configurations, while the other algorithms show varying degrees of performance.

Table 8
Comparison of the optimization results obtained by the algorithms at 0% LPSP.

Configuration	Parameter		GA	PSO	MFO	SSA	ChOA	MA	GWO	CSA	FPA	HSA
BGG/MHP/SPV/LA at 70% DOD	LCC (INR)	Best	82,934,475	**82,886,850**	**82,886,850**	**82,886,850**	**82,886,850**	**82,886,850**	**82,886,850**	**82,886,850**	**82,886,850**	**82,886,850**
		Worst	86,724,256	84,225,356	**82,886,850**	**82,886,850**	**82,886,850**	**82,886,850**	**82,886,850**	86,664,250	**82,886,850**	85,004,550
		Mean	84,010,322	83,094,606	**82,886,850**	**82,886,850**	**82,886,850**	**82,886,850**	**82,886,850**	83,559,763	**82,886,850**	83,004,412
	COE (INR/kWh)		20.37	**20.22**	**20.22**	**20.22**	**20.22**	**20.22**	**20.22**	**20.22**	**20.22**	**20.22**
	Q_{SPV}		720	**744**	**744**	**744**	**744**	**744**	**744**	**744**	**744**	**744**
	Q_{BES}		302	**281**	**281**	**281**	**281**	**281**	**281**	**281**	**281**	**281**
	CT (sec)		4010	8136	8234	5107	**3364**	5282	4856	8569	5770	6115
	SE (kWh/yr.)		311,235	318,844	318,844	318,844	318,844	318,844	318,844	318,844	318,844	318,844
BGG/MHP/SPV/LA at 80% DOD	LCC(INR)	Best	82,307,775	82,550,015	82,294,800	**82,290,225**	**82,290,225**	**82,290,225**	**82,290,225**	82,315,510	82,297,785	82,330,825
		Worst	85,627,121	88,821,026	84,805,582	**82,290,225**	**82,290,225**	83,445,512	**82,290,225**	85,445,067	88,205,624	83,325,116
		Mean	84,294,455	84,367,887	82,791,644	**82,290,225**	**82,290,225**	82,860,142	**82,290,225**	83,340,052	83,966,301	82,850,220
	COE (INR/kWh)		20.13	21.25	20.09	**20.07**	**20.07**	**20.07**	**20.07**	20.17	20.11	20.20
	Q_{SPV}		765	1001	734	**743**	**743**	**743**	**743**	772	749	788
	Q_{BES}		243	248	245	**244**	**244**	**244**	**244**	245	**244**	245
	CT (sec)		4383	5620	5543	5403	**3649**	5059	4732	6260	5104	5579
	SE (kWh/yr.)		309,897	298,119	306,452	308,386	308,386	308,386	308,386	314,028	319,920	315,422
BGG/MHP/SPV/Li-Ion at 70% DOD	LCC(INR)	Best	149,937,075	**149,906,400**	**149,906,400**	149,922,375	**149,906,400**	149,915,220	**149,906,400**	149,955,240	**149,906,400**	149,922,375
		Worst	156,734,044	150,424,237	**149,906,400**	152,376,298	**149,906,400**	152,667,030	**149,906,400**	155,247,667	151,672,840	152,550,882
		Mean	152,891,113	149,986,667	**149,906,400**	150,725,867	**149,906,400**	149,990,214	**149,906,400**	150,101,414	149,956,786	150,886,240
	COE (INR/kWh)		36.67	**36.57**	**36.57**	36.62	**36.57**	36.60	**36.57**	36.81	**36.57**	36.62
	Q_{SPV}		701	**683**	**683**	670	**683**	662	**683**	694	**683**	670
	Q_{BES}		198	**198**	**198**	199	**198**	199	**198**	199	**198**	199
	CT (sec)		3628	5221	6654	4924	**3045**	5986	5032	6686	6590	5807
	SE (kWh/yr.)		298,440	282,099	282,099	262,856	282,099	260,076	282,099	281,415	282,099	262,856
BGG/MHP/SPV/Li-Ion at 80% DOD	LCC(INR)	Best	137,775,600	137,696,925	137,696,925	137,697,975	**137,691,825**	137,786,310	137,696,540	138,237,410	137,815,525	138,054,440
		Worst	145,667,855	139,704,668	142,287,112	140,917,665	**137,691,825**	139,004,922	140,165,914	145,520,125	139,911,330	144,367,206
		Mean	142,605,672	139,099,253	138,827,219	138,410,854	**137,691,825**	137,985,054	138,885,259	139,631,119	138,255,092	138,990,058
	COE (INR/kWh)		33.86	33.60	33.60	33.61	**33.59**	33.92	33.60	34.24	33.98	34.11
	Q_{SPV}		815	657	657	680	**654**	666	656	649	672	747
	Q_{BES}		167	173	173	172	**173**	173	173	175	173	173
	CT (sec)		4837	5758	5572	5852	**4057**	6392	5167	7204	5888	6026
	SE (kWh/yr.)		288,135	263,589	263,589	269,454	262,617	264,339	263,011	261,110	268,225	271,356
BGG/MHP/SPV/NAS at 70% DOD	LCC(INR)	Best	68,797,800	**68,775,000**	**68,775,000**	**68,775,000**	**68,775,000**	**68,775,000**	**68,775,000**	68,815,740	**68,775,000**	68,789,115
		Worst	73,567,220	**68,775,000**	**68,775,000**	**68,775,000**	**68,775,000**	**68,775,000**	**68,775,000**	74,004,625	**68,775,000**	73,028,260
		Mean	69,217,164	**68,775,000**	**68,775,000**	**68,775,000**	**68,775,000**	**68,775,000**	**68,775,000**	69,600,577	**68,775,000**	69,445,012
	COE (INR/kWh)		16.85	**16.77**	**16.77**	**16.77**	**16.77**	**16.77**	**16.77**	16.96	**16.77**	16.82
	Q_{SPV}		730	**676**	**676**	**676**	**676**	**676**	**676**	736	**676**	722
	Q_{BES}		647	**648**	**648**	**648**	**648**	**648**	**648**	**648**	**648**	647
	CT (sec)		4253	5592	5245	5239	**3574**	6035	5811	6779	5505	5994
	SE (kWh/yr.)		284,412	273,359	273,359	273,359	273,359	273,359	273,359	284,977	273,359	283,704
BGG/MHP/SPV/NAS at 80% DOD	LCC(INR)	Best	**80,529,750**	**80,529,750**	**80,529,750**	**80,529,750**	**80,529,750**	80,781,955	**80,529,750**	**80,529,750**	**80,529,750**	80,957,075
		Worst	86,376,228	86,044,312	85,227,036	80,666,263	**80,529,750**	82,765,050	82,606,820	84,415,085	82,850,114	85,229,935
		Mean	82,105,445	82,198,335	81,112,903	80,587,130	**80,529,750**	80,904,616	80,992,336	82,047,068	80,911,157	82,690,033
	COE (INR/kWh)		**19.64**	**19.64**	**19.64**	**19.64**	**19.64**	19.79	**19.64**	**19.64**	**19.64**	19.95
	Q_{SPV}		**675**	**675**	**675**	**675**	**675**	688	**675**	**675**	**675**	677
	Q_{BES}		**564**	**564**	**564**	**564**	**564**	**564**	**564**	**564**	**564**	565
	CT (sec)		3924	4821	4791	4818	**3287**	5976	5904	6115	5786	5530
	SE (kWh/yr.)		291,889	273,675	273,675	273,675	273,675	295,067	273,675	273,675	273,675	268,244
BGG/MHP/SPV/Ni-Fe at 70% DOD	LCC(INR)	Best	**116,087,925**	116,135,775	**116,087,925**	**116,087,925**	**116,087,925**	**116,087,925**	**116,087,925**	**116,087,925**	116,659,095	**116,087,925**
		Worst	122,194,827	120,876,588	**116,087,925**	**116,087,925**	**116,087,925**	120,664,150	**116,087,925**	122,404,770	123,005,475	122,767,450
		Mean	119,074,449	117,199,416	**116,087,925**	**116,087,925**	**116,087,925**	116,555,087	**116,087,925**	117,884,019	118,011,788	117,347,506
	COE (INR/kWh)		**28.32**	28.47	**28.32**	**28.32**	**28.32**	**28.32**	**28.32**	**28.32**	28.75	**28.32**
	Q_{SPV}		**853**	863	**853**	**853**	**853**	**853**	**853**	**853**	867	**853**
	Q_{BES}		**787**	792	**787**	**787**	**787**	**787**	**787**	**787**	795	**787**

(*continued on next page*)

Table 8 (*continued*)

Configuration	Parameter		GA	PSO	MFO	SSA	ChOA	MA	GWO	CSA	FPA	HSA
BGG/MHP/SPV/Ni-Fe at 80% DOD	CT (sec)		3875	4751	5065	5063	**3251**	6617	4909	7025	6145	6427
	SE (kWh/yr.)		352,044	347,886	349,253	349,253	349,253	349,253	349,253	349,253	340,056	349,253
	LCC(INR)	Best	103,592,925	**103,575,375**	**103,575,375**	**103,575,375**	**103,575,375**	**103,575,375**	**103,575,375**	**103,575,375**	**103,575,375**	103,667,110
		Worst	104,806,225	**103,575,375**	**103,575,375**	**103,575,375**	**103,575,375**	**103,575,375**	**103,575,375**	105,008,656	105,724,995	105,918,275
		Mean	103,713,852	**103,575,375**	**103,575,375**	**103,575,375**	**103,575,375**	**103,575,375**	**103,575,375**	103,780,306	103,954,066	103,756,011
	COE (INR/kWh)		25.45	**25.26**	**25.26**	**25.26**	**25.26**	**25.26**	**25.26**	**25.26**	**25.26**	25.62
	Q_{SPV}		854	**836**	**836**	**836**	**836**	**836**	**836**	**836**	**836**	842
	Q_{BES}		670	**671**	**671**	**671**	**671**	**671**	**671**	**671**	**671**	672
	CT (sec)		4317	5303	5270	5300	**3616**	5059	4887	6318	6367	5705
	SE (kWh/yr.)		354,124	342,932	342,932	342,932	342,932	342,932	342,932	342,932	342,932	342,015

4.2.2. Convergence rapidity plot of the deployed algorithms

The convergence rapidity plot in Fig. 9 shows how well the algorithms find the global optimal solution. Fig. 9 indicates the minimum LCC values achieved by each algorithm at different iterations. The plot shows that the GA, SSA, PSO, FPA, CSA, HSA, GWO, MA, MFO, and ChOA reach their minimum LCC in the 69th, 61st, 56th, 55th, 49th, 47th, 44th, 35th, 34th and 26th iterations, respectively, for NAS battery configuration.

Similarly, for the LA battery configuration, the algorithms reach their minimum LCC in the 66th, 57th, 57th, 49th, 46th, 51st, 44th, 45th, 37th, and 35th iterations for GA, SSA, PSO, FPA, CSA, HSA, GWO, MA, MFO, and ChOA, respectively.

For the Ni-Fe battery configuration, the algorithms reach their minimum LCC in the 60th, 45th, 44th, 54th, 44th, 55th, 48th, 49th, 42nd, and 37th iterations for GA, SSA, PSO, FPA, CSA, HSA, GWO, MA, MFO, and ChOA, respectively.

For the Li-Ion battery configuration, the algorithms reach their minimum LCC in the 57th, 49th, 45th, 57th, 49th, 57th, 53rd, 46th, 40th, and 31st iterations for GA, SSA, PSO, FPA, CSA, HSA, GWO, MA, MFO, and ChOA, respectively.

In summary, the rankings of the algorithms for providing the least LCC solution in the minimum iterations are as follows: ChOA (1st rank), MFO (2nd rank), MA (3rd rank), CSA (4th rank), GWO (5th rank), PSO (6th rank), HSA (7th rank), SSA (8th rank), FPA (9th rank), and GA (10th rank).

4.2.3. Average computational time (CT) of deployed algorithms

The amount of time it takes to complete one run simulation by an algorithm is called computational time (CT). To examine the resilience of each algorithm after the entire simulation process is completed, the average CT of each algorithm in eight configurations is evaluated and compared to the other algorithms as explained below.

According to the results given in Table 8, the CSA algorithm is ranked tenth because it takes an average of 6870 s to complete one run simulation. The HSA ranks ninth with an average CT of 5898 s. The FPA ranks eighth with an average CT of 5895 s. The MA ranks seventh with an average CT of 5801 s. The MFO ranks sixth with an average CT of 5797 s. The PSO ranks fifth with an average CT of 5651 s. The SSA ranks fourth with an average CT of 5214 s. The GWO ranks third with an average CT of 5163 s. Whereas, GA on the other hand, has an average CT of 4154 s and is ranked second. Finally, the ChOA is ranked first because its average CT to complete one run simulation is 3481 s.

Therefore, the ChOA algorithm demonstrates the highest resilience and efficiency among the compared algorithms, as it achieves the minimum average CT to complete one run simulation.

Based on the Best, Worst, and Mean values of LCC, convergence rapidity, and average CT of algorithms, the ranking criterion has been developed and shown in Table 9. It shows that the HSA, FPA, CSA, GA, PSO, SSA, MA, MFO, GWO, and ChOA are ranked 10th, 9th, 8th, 7th, 6th, 5th, 4th, 3rd, 2nd, and 1st overall, respectively. Based on this ranking, the proposed ChOA algorithm is highly recommended for optimal sizing of the IRESs as it achieves the highest ranking among the compared algorithms.

4.3. Analysis of electric vehicle (EV) charging strategies

EVs are widely recognized as pollution-free and environmentally friendly modes of transportation. However, integrating EVs into the transportation industry necessitates careful consideration of charging infrastructure. Without a coordinated charging plan, the full potential of battery storage capacity remains untapped, and unmanaged charging can lead to increased peak demand, thereby straining the power system. Therefore, a well-planned charging approach is crucial to yield positive outcomes. Consequently, this study explores four charging strategies, namely: i) Dumb charging, ii) Battery swapping charging, iii) Smart charging, and iv) Integrated charging.

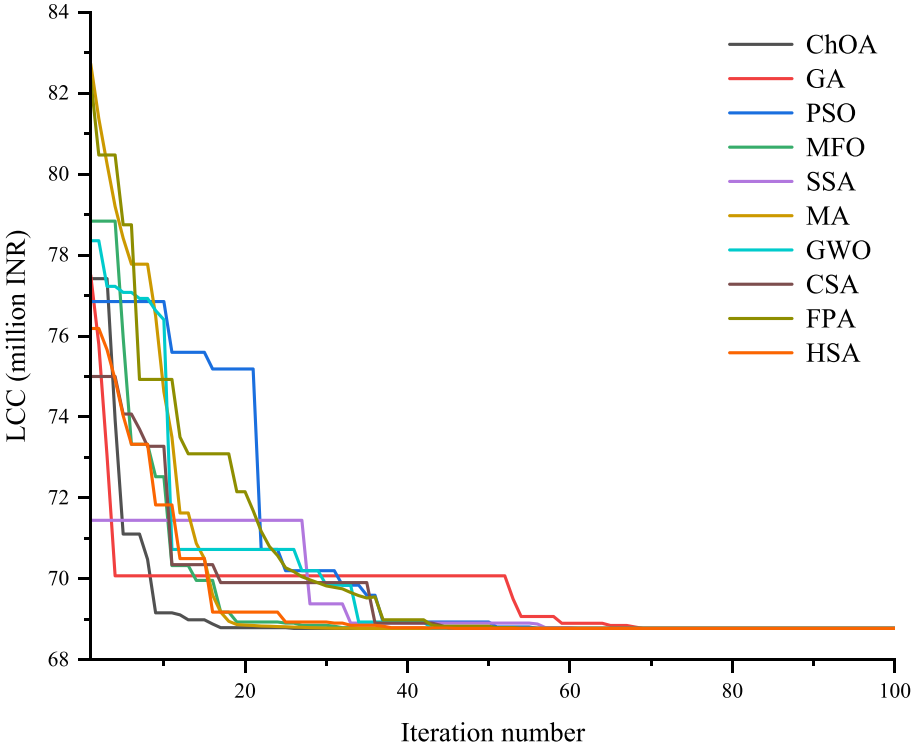

Fig. 9. Convergence rapidity plot of NAS at 70% DOD battery configured optimal IRES.

Table 9
Overall ranking criterion of applied algorithms.

Ranking criterion	GA	PSO	MFO	SSA	ChOA	MA	GWO	CSA	FPA	HSA
Best, Worst, and Mean values of LCC	7	5	3	3	1	4	2	6	5	7
Convergence rapidity	10	6	2	8	1	3	5	4	9	7
CT	2	5	6	4	1	7	3	10	8	9
Overall rank	**7**	**6**	**3**	**5**	**1**	**4**	**2**	**8**	**9**	**10**

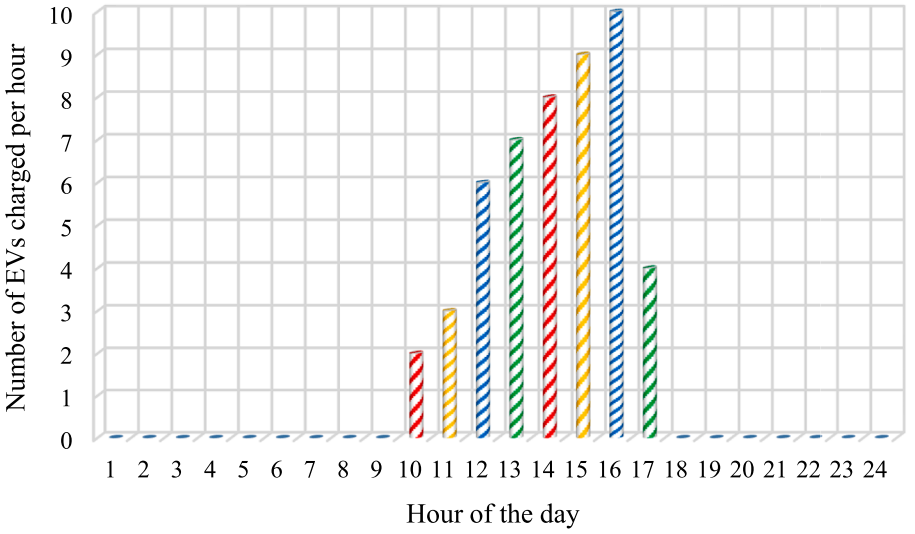

Fig. 10. Number of EVs charging per hour in the DBC strategy.

4.3.1. Dumb charging (DBC) strategy

The DBC strategy involves simply plugging in and charging EVs when they arrive home, without any advanced coordination or control. However, this strategy can lead to exceed the system's peak-load demand. Fig. 10 presents the number of EVs charging every hour for a 24-hour period, under the DBC strategy. In this strategy, the system is able to charge 49 EVs per day, utilizing only 38.83 % of the available SE. The daily utilization of SE in EV charging under the DBC strategy is

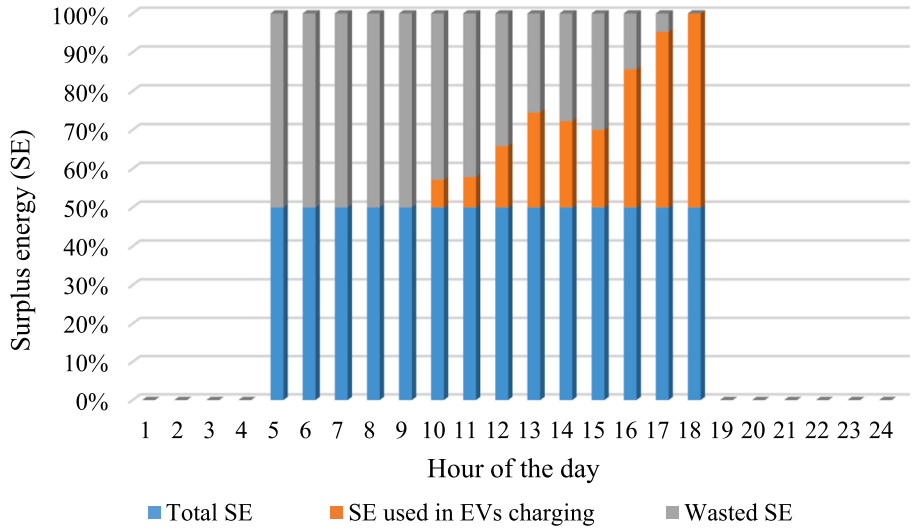

Fig. 11. Daily utilization of SE in EV charging under the DBC strategy.

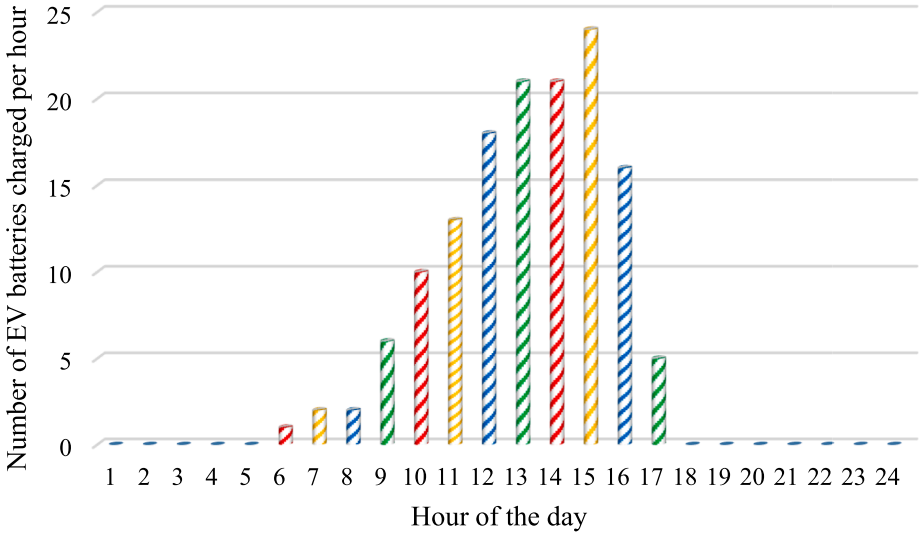

Fig. 12. Number of EVs charging per hour in the BSC strategy.

depicted in Fig. 11. Additionally, the DBC strategy result in a significant 26.88 % reduction in the total COE, while increasing the total annual energy utilization (AEU) by 36.77 %.

4.3.2. Battery swapping charging (BSC) strategy

The BSC strategy involves EV owners charging an additional battery at home whenever SE is available, irrespective of their EV arrival time. Fig. 12 illustrates the hourly EV battery charging patterns based on the availability of SE.

Under the BSC strategy, the current system is capable of energizing 139 EVs per day, utilizing 100 % of the available SE, as demonstrated in Fig. 13. However, the introduction of standby batteries leads to an increase in the total COE to consumers by 50.52 %, and the total AEU experiences a significant boost of 99.69 %.

4.3.3. Smart charging (SC) strategy

The SC strategy enables EV drivers to charge a greater number of EVs per day without incurring additional COE. This feat is achieved by smartly adjusting the departure-arrival time of EVs belonging to trip chain activities viz: goods transport, shopping/errands, gathering/functions, temple/mosque/church, etc. to maximize the utilization of SE in EVs charging. However, it is important to note that trip chains with fixed times, such as school and work/offices, cannot be altered. For other activities, the arrival times of EVs can be smartly adjusted to optimize the utilization of SE. Fig. 14 presents the new arrival times of EVs under the SC strategy.

Fig. 15 demonstrates that by utilizing 66.63 % of the SE, a total of 75 EVs can be charged per day using the SC strategy. This strategy leads to a reduction in total COE by 38.69 % while increasing the total AEU by 63.1 %. Furthermore, Fig. 16 illustrates the daily utilization of SE in EV charging under the SC strategy.

4.3.4. Integrated charging (IC) strategy

The proposed IC strategy combines elements of dumb charging, battery swapping, and smart charging to address the drawbacks of individual charging strategies while harnessing their respective benefits. The objective is to create a hybrid strategy that optimizes EV charging operations.

In the IC strategy, the departure-arrival timings of trip chain activities such as goods transport, shopping/errands, gatherings/functions, and temple/mosque/church visits are smartly adjusted, similar to the approach in the SC strategy. This allows for the efficient utilization of SE

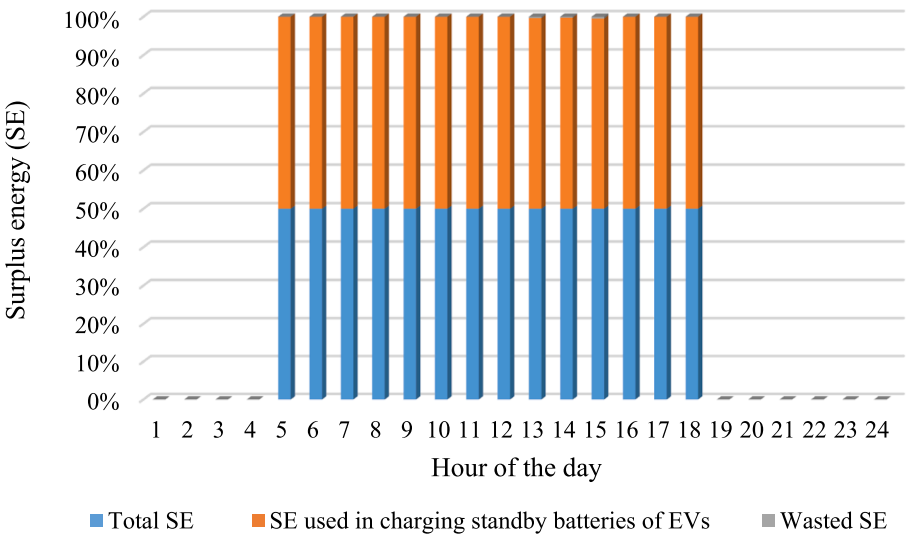

Fig. 13. Daily utilization of SE in charging standby batteries of EVs under the BSC strategy.

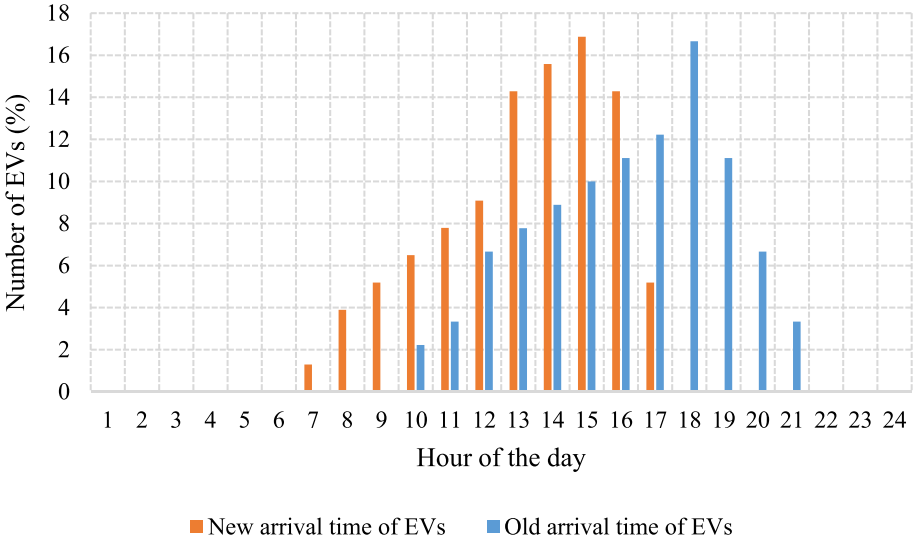

Fig. 14. The new arrival time of EVs under the SC strategy.

during EV charging. Additionally, to maximize SE utilization and enhance EV penetration, EV standby batteries are utilized to store remaining hourly available SE. Standby batteries are allocated to EVs involved in trip chains like schools and work/offices, where the trip times cannot be changed.

Fig. 17 demonstrates how the IC strategy power 134 EVs by utilizing 99.59 % of SE. Specifically, 75 EVs are charged using the SC strategy, 44 EVs using the DBC strategy, and 15 EVs using the BSC strategy. Moreover, the IC strategy reduces the total COE by 37.93 % while increasing the total AEU by 99.3 %. Fig. 18 illustrates the daily utilization of SE in EV charging under the IC strategy.

Table 10 summarizes the performance of all charging strategies. The IC strategy charges more EVs by using over 99 % of SE than the DBC and SC strategies. Additionally, it reduces total COE more than the others. The BSC strategy, on the other hand, achieves the maximum number of charged EVs, while increasing the total COE.

Performance analysis shows that the IC strategy is best for microgrid EV charging. It uses SE to charge a significant number of EVs at the lowest COE than other methods. Overall, the findings support the suitability of the IC strategy for efficient and sustainable EV charging in microgrid systems.

4.4. Emission analysis

Table 11 shows GHG emissions from the conventional grid, RE resources, and GVs under the IC strategy. The proposed IRES net CO_2 savings and tons of CO_2, CH_4, and N_2O emissions are listed. The table indicates that the proposed IRES emits 9646 tons of GHGs, 9.3 % of the conventional grid emissions. It is estimated that the IC strategy saves 94479.39 tons of GHG emissions. In addition to Table 11, Fig. 19 shows the avoided CO_2 emissions from implementing the IRES with EVs under DBC, BSC, SC, and IC strategies.

These findings underscore the positive impact of the IC strategy in reducing CO_2 emissions, promoting sustainability, and contributing to the overall decarbonization efforts associated with EV integration and RE utilization.

5. Conclusions

This study investigates the feasibility of a stand-alone integrated renewable energy system (IRES) to supply electricity for various purposes to a cluster of twelve un-electrified villages in Munsyari Block, Uttarakhand, India. This study presented a stand-alone IRES design

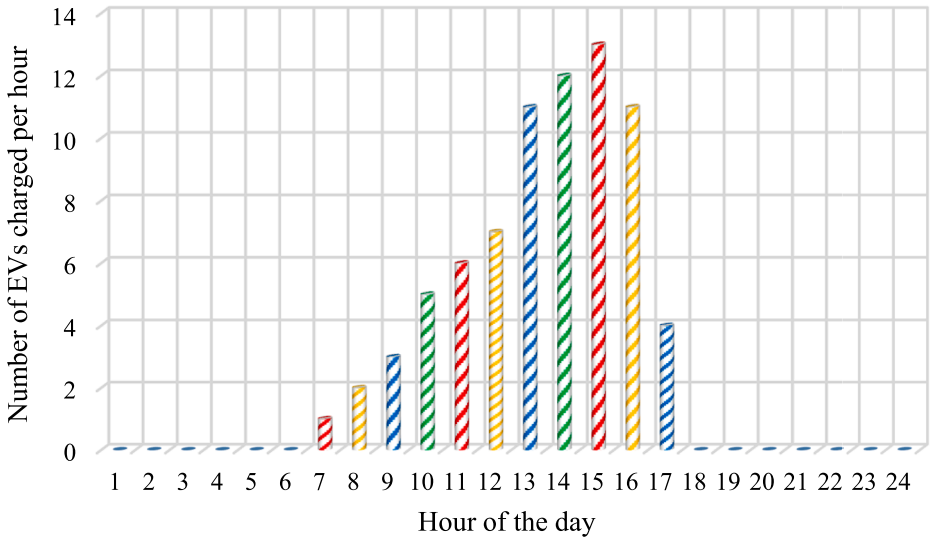

Fig. 15. Number of EVs charging every hour in the SC strategy.

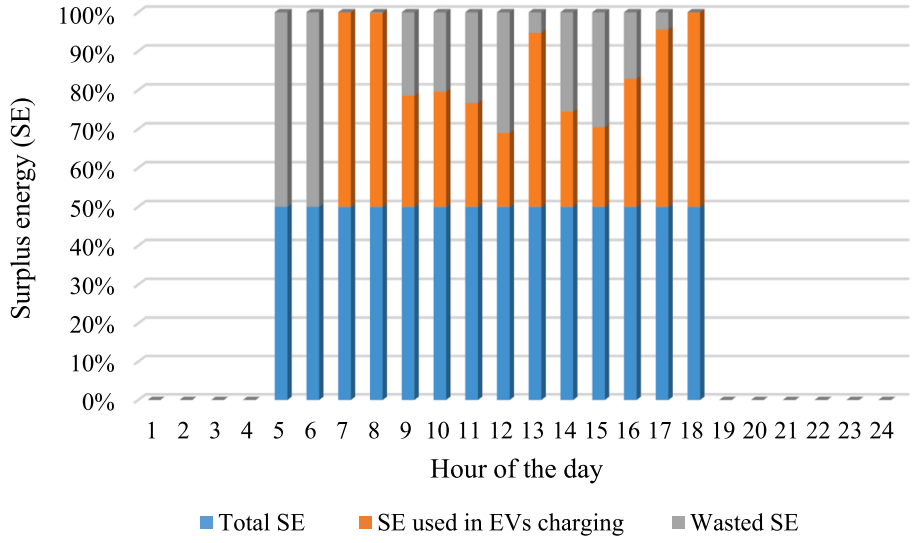

Fig. 16. Daily utilization of SE in EV charging under the SC strategy.

framework with diverse BES devices. The developed system has been optimized using the novel Chimp optimization algorithm (ChOA). Electric Vehicles (EVs) are used as dump load to consume surplus energy (SE). Finally, the optimal IRES and EVs under different charging strategies were analyzed for greenhouse gas (GHG) emission reduction. The following are the findings of the study:

(i) The study proposes the electrification of the study area using the optimal IRES configuration, including BGG/MHP/SPV/NAS at a depth of discharge (DOD) of 70 %. The cost of energy (COE) for this configuration is found 16.77 INR/kWh, and the life cycle cost (LCC) amount to 68.77 million INR.

(ii) The optimal IRES configuration includes 676 solar photovoltaic (SPV) panels with a capacity of 260 kWp, one micro-hydropower (MHP) plant with a capacity of 25 kW, one biogas generator (BGG) with a capacity of 40 kW, and 648 sodium-sulfur (NAS) batteries with a capacity of 778 kWh.

(iii) Alternative configurations, such as BGG/MHP/SPV/LA at 80 % DOD, BGG/MHP/SPV/Ni-Fe at 80 % DOD, and BGG/MHP/SPV/Li-Ion at 80 % DOD, have LCCs and COEs approximately 20 %, 50 %, and 100 % higher than the optimal configuration, respectively.

(iv) Among all the deployed algorithms, ChOA secures 1st rank in all the ranking criteria such as Best, Worst, and Mean values of LCC, convergence rapidity, and average computational time (CT) taken while searching global best results. Indicating its effectiveness in optimizing the IRES design.

(v) Among the EV charging strategies considered, the integrated charging (IC) strategy yielded the best results, enabling the charging of 134 EVs using 99.59 % of SE, and reducing the total COE to 10.57 INR/kWh.

(vi) The IC strategy achieved significant GHG emission reductions, with an overall net saving of 94,479.39 tons. The IRES alone and the IRES with EVs under various strategies avoided approximately 290.77 to 291.61 tons of CO_2 emissions.

The adopted methodology can be useful in designing IRES for other remote rural areas that are not yet electrified. However, there is room for further research into other energy storage devices such as hydrogen energy storage, pump hydro storage, or hybrid energy storage systems.

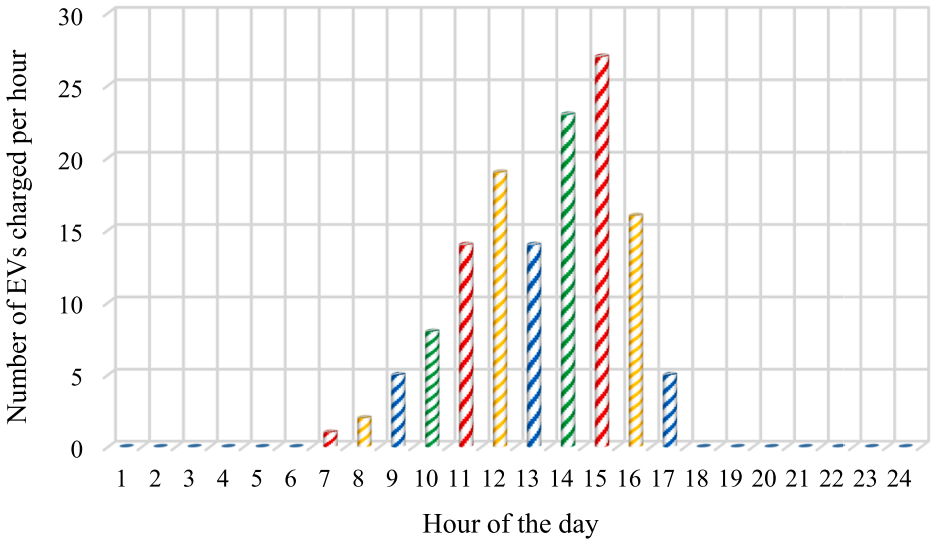

Fig. 17. Number of EVs charging per hour in the IC strategy.

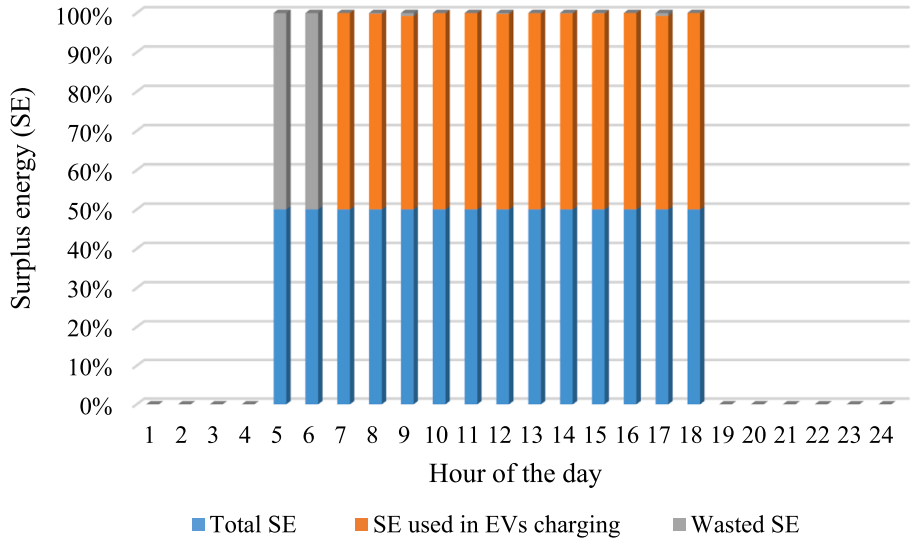

Fig. 18. Daily utilization of SE in EV charging under the IC strategy.

Table 10
Performance analysis of all the charging strategies.

Parameters	DBC strategy	BSC strategy	SC strategy	IC strategy
Charged EVs	49	139	75	**134**
Utilization of SE (%)	38.83	100	66.67	**99.59**
COE (INR/kWh)	12.22	26.85	10.27	**10.57**
Increase in AEU (%)	36.77	99.69	63.1	**99.3**

Furthermore, the performance of EVs in terms of fuel cost and carbon emissions should be compared with other vehicles such as hybrid energy vehicles and flex-fuel vehicles.

Declaration of Competing Interest

The authors declare that they have no known competing financial interests or personal relationships that could have appeared to influence the work reported in this paper.

Table 11
The overall CO_2 emission.

GHG emission (tons)	Grid	SPV	MHP	BGG	IC	Net saving
CO_2	320.53	22.25	1.73	5.78	0.84	291.61
CH_4	8013.35	556.32	43.41	144.54	21.00	7290.07
N_2O	95519.20	6631.36	517.56	1722.91	250.35	86897.71
Total GHG	103853.09	7209.93	562.72	1873.23	272.20	94479.39

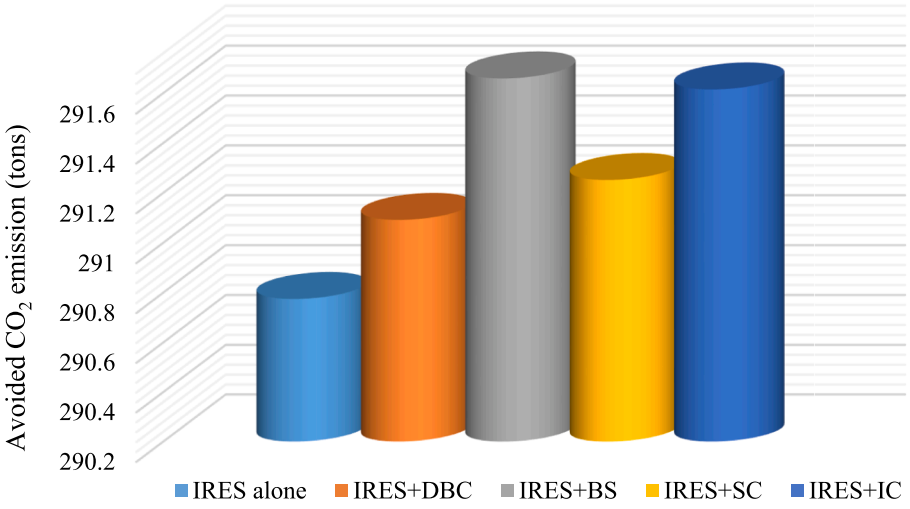

Fig. 19. Total CO_2 emission avoided by the IRES with EVs under different charging strategies.

Acknowledgment

The first author wishes to express gratitude to the Ministry of Education (MOE), Government of India, for giving financial assistance in the form of a fellowship for the research work.

References

[1] R. Pachauri, R. Singh, A. Gehlot, R. Samakaria, S. Choudhury, Experimental analysis to extract maximum power from PV array reconfiguration under partial shading conditions, Eng. Sci. Technol. Int. J. 22 (1) (2019) 109–130, https://doi.org/10.1016/j.jestch.2017.11.013.

[2] E. Biyik, et al., A key review of building integrated photovoltaic (BIPV) systems, Eng. Sci. Technol. Int. J. 20 (3) (2017) 833–858, https://doi.org/10.1016/j.jestch.2017.01.009.

[3] "Global status report." [Online]. Available: https://www.ren21.net/gsr-2023/.

[4] T.R. Ayodele, A.S.O. Ogunjuyigbe, K.O. Akpeji, O.O. Akinola, Prioritized rule based load management technique for residential building powered by PV/battery system, Eng. Sci. Technol. Int. J. 20 (3) (2017) 859–873, https://doi.org/10.1016/j.jestch.2017.04.003.

[5] D. Kumar, H.D. Mathur, S. Bhanot, R.C. Bansal, Modeling and frequency control of community micro-grids under stochastic solar and wind sources, Eng. Sci. Technol. Int. J. 23 (5) (2020) 1084–1099, https://doi.org/10.1016/j.jestch.2020.02.005.

[6] M.S. Alam, F.S. Al-Ismail, S.M. Rahman, M. Shafiullah, M.A. Hossain, Planning and protection of DC microgrid: A critical review on recent developments, Eng. Sci. Technol. Int. J. 41 (2023), 101404, https://doi.org/10.1016/j.jestch.2023.101404.

[7] D. Sadeghi, A. Hesami Naghshbandy, S. Bahramara, Optimal sizing of hybrid renewable energy systems in presence of electric vehicles using multi-objective particle swarm optimization, Energy 209 (2020), 118471, https://doi.org/10.1016/j.energy.2020.118471.

[8] A. Dogan, Optimum sitting and sizing of WTs, PVs, ESSs and EVCSs using hybrid soccer league competition-pattern search algorithm, Eng. Sci. Technol. Int. J. 24 (3) (2021) 795–805, https://doi.org/10.1016/j.jestch.2020.12.007.

[9] M.M. Samy, A. Emam, E. Tag-Eldin, S. Barakat, Exploring energy storage methods for grid-connected clean power plants in case of repetitive outages, J. Storage Mater. 54 (2022), 105307, https://doi.org/10.1016/j.est.2022.105307.

[10] S.S. Reddy, Optimal power flow with renewable energy resources including storage, Electr. Eng. 99 (2) (2017) 685–695, https://doi.org/10.1007/s00202-016-0402-5.

[11] J.A. Momoh, S.R. Salkuti, Feasibility of Stochastic Voltage/VAr Optimization Considering Renewable Energy Resources for Smart Grid, Int. J. Emerg. Electr. Power Syst. 17 (3) (2016) 287–300, https://doi.org/10.1515/ijeeps-2016-0009.

[12] A. Fatih Güven, M. Mahmoud Samy, Performance analysis of autonomous green energy system based on multi and hybrid metaheuristic optimization approaches, Energ. Conver. Manage. 269 (2022), 116058, https://doi.org/10.1016/j.enconman.2022.116058.

[13] A. Chauhan, R.P. Saini, A review on Integrated Renewable Energy System based power generation for stand-alone applications: Configurations, storage options, sizing methodologies and control, Renew. Sustain. Energy Rev. 38 (2014) 99–120.

[14] S. Turkdogan, Design and optimization of a solely renewable based hybrid energy system for residential electrical load and fuel cell electric vehicle, Eng. Sci. Technol. Int. J. 24 (2) (2021) 397–404, https://doi.org/10.1016/j.jestch.2020.08.017.

[15] Q. Hassan, Evaluation and optimization of off-grid and on-grid photovoltaic power system for typical household electrification, Renew. Energy 164 (2021) 375–390.

[16] C. Mokhtara, B. Negrou, A. Bouferrouk, Y. Yao, N. Settou, M. Ramadan, Integrated supply–demand energy management for optimal design of off-grid hybrid renewable energy systems for residential electrification in arid climates, Energ. Conver. Manage. 221 (2020), 113192.

[17] A.M. Patel, S.K. Singal, Optimal component selection of integrated renewable energy system for power generation in stand-alone applications, Energy 175 (2019) 481–504.

[18] F.A. Khan, N. Pal, S.H. Saeed, Optimization and sizing of SPV/Wind hybrid renewable energy system: A techno-economic and social perspective, Energy 233 (2021), 121114, https://doi.org/10.1016/j.energy.2021.121114.

[19] M. S. Javed, T. Ma, J. Jurasz, and J. Mikulik, "A hybrid method for scenario-based techno-economic-environmental analysis of off-grid renewable energy systems," *Renewable and Sustainable Energy Reviews*, vol. 139, no. December 2020, p. 110725, 2021, doi: 10.1016/j.rser.2021.110725.

[20] L. Al-Ghussain, A. Darwish Ahmad, A. M. Abubaker, and M. A. Mohamed, "An integrated photovoltaic/wind/biomass and hybrid energy storage systems towards 100% renewable energy microgrids in university campuses," *Sustainable Energy Technologies Assessments*, vol. 46, no. December 2020, p. 101273, 2021, doi: 10.1016/j.seta.2021.101273.

[21] F. Kahwash, A. Maheri, K. Mahkamov, Integration and optimisation of high-penetration Hybrid Renewable Energy Systems for fulfilling electrical and thermal demand for off-grid communities, Energy Convers. Manage. 236 (2021), 114035, https://doi.org/10.1016/j.enconman.2021.114035.

[22] A. Shukla, J.A. Momoh, Pseudo inspired gravitational search algorithm for optimal sizing of grid with integrated renewable energy and energy storage, J. Storage Mater. 38 (2021), 102565, https://doi.org/10.1016/j.est.2021.102565.

[23] H. Tao F.W. Ahmed H. Abdalqadir kh ahmed, M. Latifi, H. Nakamura, and Y. Li, Hybrid whale optimization and pattern search algorithm for day-ahead operation of a microgrid in the presence of electric vehicles and renewable energies Journal of Cleaner Production vol. 308, no. April 2021 127215 10.1016/j.jclepro.2021.127215.

[24] Q. Guo, S. Nojavan, S. Lei, X. Liang, Economic-environmental analysis of renewable-based microgrid under a CVaR-based two-stage stochastic model with efficient integration of plug-in electric vehicle and demand response, Sustain. Cities Soc. 75 (2021), 103276, https://doi.org/10.1016/j.scs.2021.103276.

[25] I. AlHajri, A. Ahmadian, and A. Elkamel, "Stochastic day-ahead unit commitment scheduling of integrated electricity and gas networks with hydrogen energy storage (HES), plug-in electric vehicles (PEVs) and renewable energies," *Sustainable Cities and Society*, vol. 67, no. December 2020, p. 102736, 2021, doi: 10.1016/j.scs.2021.102736.

[26] S. Zeynali, N. Nasiri, M. Marzband, S.N. Ravadanegh, A hybrid robust-stochastic framework for strategic scheduling of integrated wind farm and plug-in hybrid electric vehicle fleets, Appl. Energy 300 (2021), 117432, https://doi.org/10.1016/j.apenergy.2021.117432.

[27] A. Alsharif, C. W. Tan, R. Ayop, K. Y. Lau, and A. M. d. Dobi, "A rule-based power management strategy for Vehicle-to-Grid system using antlion sizing optimization," *Journal of Energy Storage*, vol. 41, no. April, p. 102913, 2021, doi: 10.1016/j.est.2021.102913.

[28] D. Bogdanov, A. Gulagi, M. Fasihi, C. Breyer, Full energy sector transition towards 100% renewable energy supply: Integrating power, heat, transport and industry sectors including desalination, Appl. Energy 283 (2021), 116273, https://doi.org/10.1016/j.apenergy.2020.116273.

[29] Z. Xiaoluan, H. Farajian, W. Xifeng, M. Latifi, K. Ohshima, Scheduling of renewable energy and plug-in hybrid electric vehicles based microgrid using hybrid crow-Pattern search method, J. Storage Mater. (2021), 103605, https://doi.org/10.1016/j.est.2021.103605.

[30] N.F. Alshammari, M.M. Samy, S. Barakat, Comprehensive Analysis of Multi-Objective Optimization Algorithms for Sustainable Hybrid Electric Vehicle

Charging Systems, Mathematics 11 (7) (2023) pp, https://doi.org/10.3390/math11071741.
[31] S.R. Salkuti, Optimal operation of microgrid considering renewable energy sources, electric vehicles and demand response, E3S Web Conference 87 (201) (2019) 9, https://doi.org/10.1051/e3sconf/20198701007.
[32] M. Khishe, M.R. Mosavi, Chimp optimization algorithm, Expert Syst. Appl. 149 (2020), 113338.
[33] R.J. Kuo, M.N. Alfareza, T.P.Q. Nguyen, "Genetic based density peak possibilistic fuzzy c-means algorithms to cluster analysis- a case study on customer segmentation, Eng. Sci. Technol. Int. J. 47 (2023), 101525, https://doi.org/10.1016/j.jestch.2023.101525.
[34] S. Tyagi, P. Kumar, A. Kumar, Advancements in performance of zinc oxide / carbon quantum dots based photovoltaic trigeneration system using genetic algorithm and particle swarm optimization, Sustain. Energy Technol. Assess. 60 (2023), 103501, https://doi.org/10.1016/j.seta.2023.103501.
[35] C.C.W. Chang, et al., Moth flame optimization for the maximum power point tracking scheme of photovoltaic system under partial shading conditions, Energy Rep. 9 (2023) 374–379, https://doi.org/10.1016/j.egyr.2023.09.026.
[36] M.H. Sulaiman, Z. Mustaffa, "An application of improved salp swarm algorithm for optimal power flow solution considering stochastic solar power generation", e-Prime - Advances in Electrical Engineering, Electron. Energy 5 (2023), 100195, https://doi.org/10.1016/j.prime.2023.100195.
[37] J. Li, et al., Optimal planning of Electricity-Hydrogen hybrid energy storage system considering demand response in active distribution network, Energy 273 (2023), 127142, https://doi.org/10.1016/j.energy.2023.127142.
[38] İ. Yazıcı and E. K. Yaylacı, "Modified grey wolf optimizer based MPPT design and experimentally performance evaluations for wind energy systems," *Engineering Science and Technology, an International Journal*, vol. 46, no. March, 2023, doi: 10.1016/j.jestch.2023.101520.
[39] Y. W. Koholé, C. A. Wankouo Ngouleu, F. C. V. Fohagui, and G. Tchuen, "Quantitative techno-economic comparison of a photovoltaic/wind hybrid power system with different energy storage technologies for electrification of three remote areas in Cameroon using Cuckoo search algorithm," *Journal of Energy Storage*, vol. 68, no. February, 2023, doi: 10.1016/j.est.2023.107783.
[40] H. Zhang, J. Gao, L. Kang, Y. Zhang, L. Wang, K. Wang, State of health estimation of lithium-ion batteries based on modified flower pollination algorithm-temporal convolutional network, Energy 283 (2023), 128742, https://doi.org/10.1016/j.energy.2023.128742.
[41] V. Pandiya Raj, M. Duraipandian, "Energy conservation using PISAE and cross-layer-based opportunistic routing protocol (CORP) for wireless sensor network, Eng. Sci. Technol. Int. J. 42 (2023), 101411, https://doi.org/10.1016/j.jestch.2023.101411.
[42] "Census of India." https://censusindia.gov.in/2011census/Listofvillagesandtowns.aspx (accessed Jan. 26, 2023).
[43] "Uttarakhand Tehsilwise and Districtwise Livestock Census." Accessed: Jan. 29, 2023. [Online]. Available: https://dahd.nic.in/documents/statistics/livestock-census.
[44] M. Ramesh, R.P. Saini, Dispatch strategies based performance analysis of a hybrid renewable energy system for a remote rural area in India, J. Clean. Prod. 259 (2020), 120697.
[45] A. Chauhan, R.P. Saini, Discrete harmony search based size optimization of Integrated Renewable Energy System for remote rural areas of Uttarakhand state in India, Renew. Energy 94 (2016) 587–604.
[46] H. Liang, Z. Lee, G. Li, A Calculation Model of Charge and Discharge Capacity of Electric Vehicle Cluster Based on Trip Chain, IEEE Access 8 (2020) 142026–142042, https://doi.org/10.1109/ACCESS.2020.3014160.
[47] S. Sachan, S. Deb, S.N. Singh, Different charging infrastructures along with smart charging strategies for electric vehicles, Sustain. Cities Soc. vol. 60, no. May (2020), 102238, https://doi.org/10.1016/j.scs.2020.102238.
[48] Q. Wu *et al.*, "Driving Pattern Analysis for Electric Vehicle (EV) Grid Integration Study," pp. 1–6, 2011, doi: 10.1109/isgteurope.2010.5751581.
[49] M. Li, Y. Ahad, "A novel real-time pricing for optimal DRP, considering price elasticity, and charging control methods of PHEV integrated with smart grids, using GMO algorithm, Eng. Sci. Technol. Int. J. 47 (2023), 101538, https://doi.org/10.1016/j.jestch.2023.101538.
[50] D.S. Kourkoumpas, G. Benekos, N. Nikolopoulos, S. Karellas, P. Grammelis, E. Kakaras, A review of key environmental and energy performance indicators for the case of renewable energy systems when integrated with storage solutions, Appl. Energy 231 (September) (2018) 380–398, https://doi.org/10.1016/j.apenergy.2018.09.043.
[51] N. Singh, T. Mishra, R. Banerjee, Emission inventory for road transport in India in 2020: framework and post facto policy impact assessment, Environ. Sci. Pollut. Res. (2021) 1–31, https://doi.org/10.1007/s11356-021-17238-3.
[52] N. Alshammari, J. Asumadu, Optimum unit sizing of hybrid renewable energy system utilizing harmony search, Jaya and particle swarm optimization algorithms, Sustain. Cities Soc. 60 (2020), 102255, https://doi.org/10.1016/j.scs.2020.102255.
[53] "CO2 Baseline Database for the Indian Power Sector." Accessed: May 06, 2023. [Online]. Available: https://cea.nic.in/?lang=en&s=CO2+database.
[54] D. Weisser, A guide to life-cycle greenhouse gas (GHG) emissions from electric supply technologies, Energy 32 (9) (2007) 1543–1559, https://doi.org/10.1016/j.energy.2007.01.008.
[55] A.H. Elbatran, O.B. Yaakob, Y.M. Ahmed, H.M. Shabara, Operation, performance and economic analysis of low head micro-hydropower turbines for rural and remote areas: A review, Renew. Sustain. Energy Rev. 43 (2015) 40–50, https://doi.org/10.1016/j.rser.2014.11.045.
[56] A. Maleki, Design and optimization of autonomous solar-wind-reverse osmosis desalination systems coupling battery and hydrogen energy storage by an improved bee algorithm, Desalination 435 (March) (2018), https://doi.org/10.1016/j.desal.2017.05.034.
[57] R. Mishra, S.K. Chaulya, G.M. Prasad, S.K. Mandal, G. Banerjee, Design of a low cost, smart and stand-alone PV cold storage system using a domestic split air conditioner, J. Stored Prod. Res. 89 (2020), 101720, https://doi.org/10.1016/j.jspr.2020.101720.